STScI | SPACE TELESCOPE SCIENCE INSTITUTE

Instrument Science Report STIS 2022-02(v1)

STIS CCD & MAMA Full-field Sensitivity & its Time Dependence

L. Prichard[1]

[1] Space Telescope Science Institute, Baltimore, MD

28 April 2022

ABSTRACT

*The three detectors on STIS, one CCD and two MAMAs, are subject to time-dependent sensitivity (TDS) changes on both short- and long-timescales. These variations are corrected for in the STIS calibration pipeline (*CALSTIS*) with TDS models derived from spectroscopic data. In this analysis, we measure residual TDS trends in the data after these corrections are applied. We update the analysis presented in STIS ISR 2013-02 (using data from 1997 to 2012) with the goal of tracking the efficacy of these TDS corrections for data taken up to 2022. We measure aperture photometry of sources in standard stellar fields (NGC 5139 for the CCD, NGC 6681 for the MAMAs) and derive magnitude trends for each star with time. We then determine overall residual TDS effects for each detector, and by filter for the NUV and FUV MAMAs (with data in three filters each). We find roughly consistent results to those from STIS ISR 2013-02 measured over the same time period, that show magnitude trends are within the* $\sim 1\%$ *STIS flux calibration accuracy. We observe stronger negative magnitude trends (i.e., sources appearing brighter with time) when including more recent data. This implies that the TDS models are over correcting the data which could mean that the loss of imaging sensitivity is slowing at a more rapid rate than the spectroscopic TDS models predict, as determined independently for all three STIS detectors. We also measure point spread functions for each image and find no significant trends in their full-width-half-max values with time for any detector.*

Operated by the Association of Universities for Research in Astronomy, Inc., for the National Aeronautics and Space Administration.

Contents

1. Introduction

The Space Telescope Imaging Spectrograph (STIS) instrument on board the *Hubble Space Telescope* (HST) has three detectors spanning optical, near-ultraviolet (NUV) and far-UV (FUV) wavelengths. The sensitivity of the charge-coupled device (CCD) detector and two multi-anode microchannel array (MAMA) detectors is known to decrease with time. These long-term time-dependent sensitivity (TDS) trends, and shorter-term temperature variations that affect the CCD detector, are modeled, and corrected for in the STIS data pipeline (CALSTIS). The correction coefficients are stored in the TDS reference file that is applied to the data. Details of the TDS model derivations are described in STIS Instrument Science Reports (ISRs) 2004-04 (Stys et al., 2004) and 2017-06 (Carlberg & Monroe, 2017).

In the case of STIS imaging data taken with the CCD, NUV MAMA and FUV MAMA detectors, the TDS correction models are calibrated with spectroscopic data. TDS trends measured from the spectroscopic L-modes that are applied to the imaging data vary by 10–15% across the lifetime of STIS (e.g., ISR 2017-06). The sensitivity loss of the detectors is also slowing with time as expected due to their degradation. The goal of this analysis is to track if there are any residual TDS trends that exist in the

data after the CALSTIS calibrations are applied. This is done to test the efficacy of the existing TDS models calibrated on older spectroscopic data to correct imaging data.

This analysis was last performed 10 years ago and is presented in STIS ISR 2013-02 (Roman-Duval & Proffitt, 2013). Throughout this ISR, we adopt the latest photometry packages now available with Python while sticking as close as possible to the methodology presented in ISR 2013-02 (that used IDL routines) so we can accurately compare results. The key findings of ISR 2013-02 showed that the residual trends after the TDS models were applied were within the 1% flux calibration accuracy for STIS (e.g., Bohlin et al., 2019) and well within the $\sim 5\%$ quoted STIS photometric accuracy (STIS Instrument Handbook[1]). In this analysis over the same 15-year time period as ISR 2013-02 (1997 to 2012), we also find that the residual flux variations are also within $\sim 1\%$.

We see larger overall residual trends per detector when including all data available from 1997 to 2022, up to $\sim 1.4\%$ flux change for the CCD, and even larger residuals for the FUV MAMA ($\sim 3.53\%$). More significant is the increasingly negative magnitude residual trends (stars appearing brighter with time) for all three detectors which implies that the current TDS models are over correcting the data. This may indicate a more rapid slowdown in the imaging sensitivity loss of all STIS detectors (as measured independently from each) relative to the slowdown predicted by the spectroscopic TDS models.

We summarize the properties of the data used in this analysis in Section 2 and the details of the charge transfer inefficiency (CTI) corrections applied to the CCD data in Section 3. The image alignment is described in Section 4 and the source detection in Section 5. The creation of point spread functions (PSFs) for each image and aperture photometry details are in Sections 6 and 7 respectively. We present our main results in Section 8, discuss these results and key conclusions in Section 9, and provide recommendations for next steps in Section 10.

2. Data

2.1 CCD Observations

The CCD data for the full-field sensitivity monitoring (FFSM) analysis are of the standard star field NGC 5139. The CCD data span 25 years and are taken yearly between 1997 and 2022, excluding 2004 to after Servicing-Mission 4 (SM4) in 2009 when STIS was repaired. We identify the proposal IDs (PIDs) from the STIS Calibration web page[2] and retrieve the associated data from MAST with ASTROQUERY (Ginsburg et al. 2019). The data are from PIDs 7079, 7639, 8056, 8416, 8847, 8912, 9622, 10028, 11854, 12409, 12770, 13139, 13542, 13989, 14421, 14827, 14968, 15556, 15745, 16347, 16555 (Cycle 29). The previous analysis from ISR 2013-02 ran

[1] https://hst-docs.stsci.edu/stisihb

[2] https://www.stsci.edu/hst/instrumentation/stis/calibration

up to 2012, PID 12770 (Cycle 19).

All images are taken with the unfiltered 50CCD aperture and as done in ISR 2013-02, only those images taken with the default science amplifier D with CCDGAIN = 4 to minimize saturation are used for analysis. Most CCD images are taken with either 10 s and 60 s total exposure times with 2 s and 30 s per read. See Table 4 in Appendix A for a summary of all CCD exposures used for analysis and their properties. The CCD data are fully calibrated and are dark- and bias-subtracted, flat-fielded, sky-subtracted, summed individual cosmic-ray (CR) split images with CR-rejection and distortion correction (sx2.fits files).

2.2 MAMA Observations

The MAMA observations for the FFSM analysis are of the globular cluster NGC 6681. The NUV and FUV MAMA data span 25 years, taken yearly from 1997 to 2022 (excluding 2004 to after SM4 in 2009). The PIDs used in this analysis are 7080, 7132, 7720, 7788, 8425, 8858, 8918, 9623, 10032, 11856, 12413, 12774, 13144, 13547, 13993, 14428, 14832, 14971, 15560, 15749, 16351, 16554 (up to Cycle 29). The previous FFSM analysis in ISR 2013-02 for the MAMAs ran up to 2012, PID 12774 (Cycle 19). PID 8422 mentioned in ISR 2013-02 only has one exposure from each detector of NGC 6681 and it is in the 52X2 filter that is not used in this analysis so we do not include it.

For the NUV MAMA detector, data observed in the F25SRF2, F25QTZ, and F25CN182 filters are used for analysis. The FUV MAMA data used for analysis are taken in the 25MAMA (clear), F25QTZ, and F25SRF2 filters. See Tables 5 and 6 in Appendix A for a summary of all NUV and FUV exposures and their properties respectively. The NUV images were taken with mostly 300 s exposures, while the FUV data have a wider spread of exposure times with 400 s being the most common.

The NUV and FUV MAMA data are fully calibrated and are dark- and bias-subtracted, flat-fielded, sky-subtracted, and distortion corrected (x2d.fits files). For the previous analysis in ISR 2013-02, geometric distortion was not yet available for the FUV images and they required reprocessing ahead of analysis. Since then, a newer distortion model described in STIS ISR 2018-02 (Sohn 2018) was applied to these data as standard. Therefore, no additional reprocessing is required for these data and the MAMA images were taken directly from MAST.

3. CCD CTI Corrections

The transfer of charge across CCD detectors while it is being read out is not efficient. The charge loss needs to be corrected for, and there are currently two methods for applying this CTI correction to STIS data. The previously available method, and that adopted for the analysis in ISR 2013-02, is that described in Goudfrooij & Bohlin 2006, Goudfrooij et al. 2006.

The code for this original empirical CTI correction, CTESTIS[3], is available in the STISTOOLS package. It takes inputs of net counts for a source (background subtracted), a sky background estimate, and the y-position on the detector (since CTI effects worsen furthest from the readout). The sky background is measured from individual cosmic-ray split, bias- and dark-subtracted, and flat-fielded images (flt.fits) that have not had any sky subtracted. The net counts measured from the science images (sx2.fits) are then scaled to the exposure time of the split image (e.g., if `CRSPLIT=5`, the counts are divided by five). The code then generates a magnitude correction (Δm) to be applied to the derived source magnitude. This correction was tested on pre-SM4 data (taken up to 2004) and can be applied to all STIS data.

The newer method is a pixel-based correction applied directly to the images themselves with the STIS_CTI code[4]. This code is based on the work of Anderson & Bedin, 2010 with parameters calibrated to STIS data (work done by Lockwood et al., see STIS ISR 2015-04, Biretta et al., 2015 and references therein). This code produces fully-calibrated CTI corrected images (s2c.fits) ready for analysis. This improved method of CTI correction can only be applied to data taken on primary science amplifier D (as used for analysis) and post-SM4 data, which are around half the available CCD data.

Table 4 shows a summary of all the CCD exposures used for this analysis. Those taken post-SM4 have an asterisk after their name to show which of those can be corrected with the pixel-based code. The CCD data with the older empirical CTI correction are used for the primary FFSM analysis as they span the full time period and can be more closely compared to ISR 2013-02. The pixel-based CTI corrected CCD images are analyzed here in addition to the main FFSM analysis (labeled the 'CCD CTI' results throughout). A detailed comparison of the two CTI correction methods is the focus of STIS ISR 2022-03 (Prichard, 2022b).

4. Image Alignment

To align the images to sub-pixel accuracy, the TWEAKREG routine from DrizzlePac (Gonzaga et al. 2012, Hoffmann et al. 2021)[5] is used. The previous analysis relied on several IDL routines and multiple steps to achieve sufficiently accurate alignment for aperture photometry. For this analysis, we use only Python routines and align the images onto a reference image in a single step to this accuracy with TWEAKREG. We use the same reference images as used in ISR 2013-02: obat01050_sx2.fits for the CCD, corresponding obat01050_s2c.fits for the pixel-based CTI corrected CCD image (from PID 11854), obav01v9q_x2d.fits for the NUV MAMA and obav01w4q_x2d.fits for the FUV MAMA (from PID 11856). Position, rotation, and linear stretch information

[3] https://stistools.readthedocs.io/en/latest/ctestis.html

[4] https://www.stsci.edu/hst/instrumentation/stis/data-analysis-and-software-tools/pixel-based-cti

[5] https://drizzlepac.readthedocs.io/en/latest/index.html

is applied to the WCS header keywords with TWEAKREG, but the STIS geometric distortion corrections remain unchanged.

The IDCSCALE header keyword, corresponding to the default plate scale of the detector, needs to be added to the STIS images for TWEAKREG to run on them (CCD 0.05072, NUV MAMA 0.0246037, FUV MAMA 0.024395). Finding the optimum TWEAKREG parameters to best align the data for each detector and set of image properties requires testing and can change with time as reference files and software are updated. The parameters found to be most valuable for aligning the images for this analysis were the threshold, minobj, peakmax, use_sharp_round=True, conv_width and searchrad. We refer the readers to the DrizzlePac and TWEAKREG documentation[6] for more information on each of the possible alignment parameters. Tips and tricks for testing TWEAKREG parameters for STIS imaging are also available in a new STIS DrizzlePac Jupyter Notebook[7].

We align all the post-SM4 CCD data (i.e., all the pixel-based CTI images) and all the CCD images spanning 25 years apart from two that are failed exposures with shorter duration (o69901010 and o69901020, also omitted in ISR 2013-02). We align all of the NUV images and all but three FUV MAMA images due to their larger offsets from the reference image and fewer sources available for matching (o46h01cwq, o46h03kuq, o5in01tdq, also omitted in ISR 2013-02). We remove two additional NUV MAMA images from the analysis that have poor tracking resulting in heavily distorted sources (ocrk01z9q, ocrk01zbq).

Using TWEAKREG, we successfully align the CCD images (65 pixel-based CTI corrected and 102 non-CTI corrected images, including the reference image) to an average accuracy of $\sim$ 0.1–0.2 pix and the MAMA data (204 images for the NUV and 224 for the FUV, including the reference images) to $\sim$ 0.2–0.5 pix accuracy. This accuracy is sufficient for performing aperture photometry on these images with no further adjustments to their alignment. See Tables 4, 5 and 6 for a summary of aligned image properties used in this analysis, with the reference images indicated by † symbols.

5. Source Detection & Catalogs

We use routines from the Python PHOTUTILS package (Bradley et al., 2020) for source finding and photometry. To identify an initial list of sources in the reference images, we use the DAOSTARFINDER routine. Basic sigma-clipped statistics are measured from each reference image (mean, median, standard deviation) and used as inputs to the DAOSTARFINDER routine. The statistics are used to approximate the sky background and corresponding threshold values used for identifying source peaks.

We run the DAOSTARFINDER routine on the reference images of each detector with the median sky background subtracted and use different parameters for each

[6] https://drizzlepac.readthedocs.io/en/latest/tweakreg.html

[7] https://github.com/spacetelescope/STIS-Notebooks, https://www.stsci.edu/hst/instrumentation/stis/data-analysis-and-software-tools

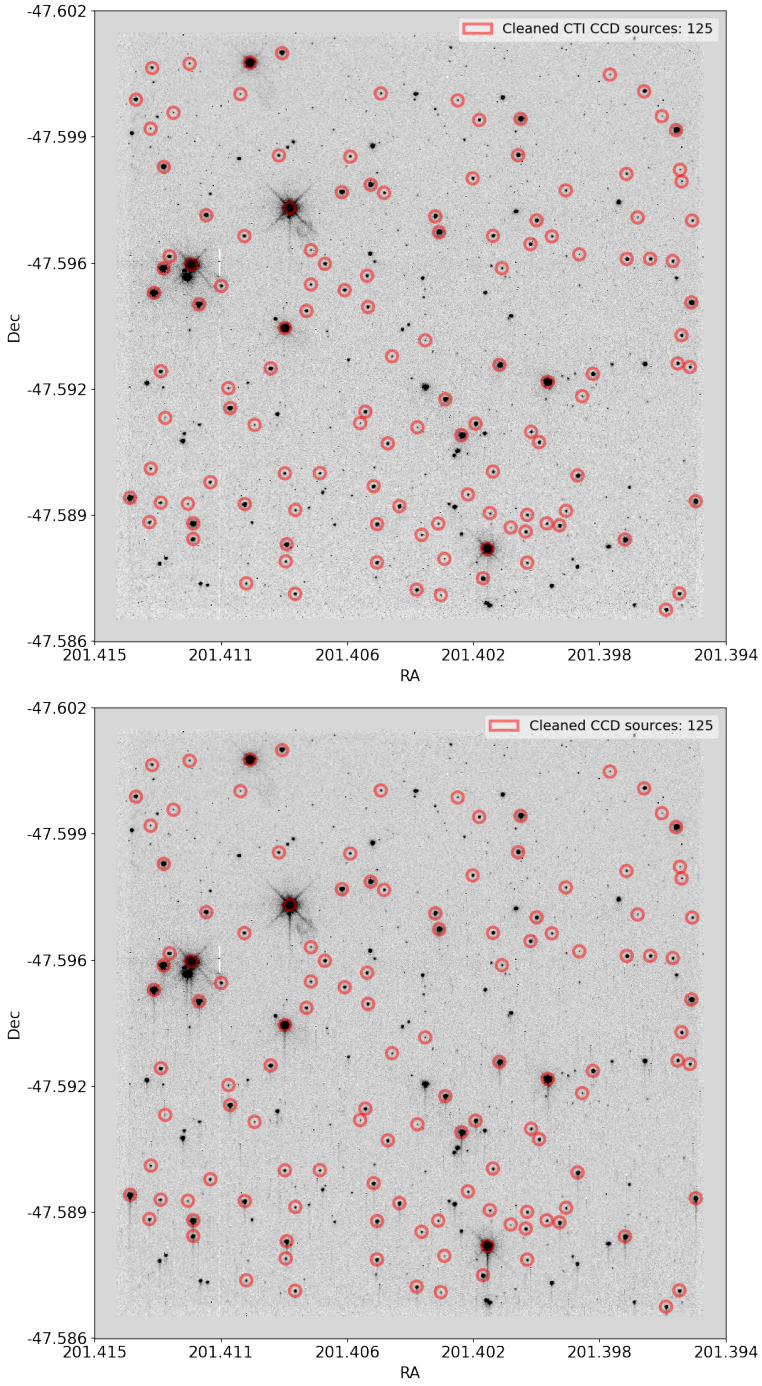

Figure 1. Cleaned list of 125 sources (red circles) identified on the CCD reference images (obat01050) of NGC 5139. Stars with close sources (within $0.8''$), contamination, or significant asymmetry were removed from the list. The same sources identified on the CCD CTI image were used for the non-CTI corrected CCD images to ensure the trails caused by CTI did not affect the source centering or background. *Top:* CCD image CTI corrected with the pixel-based code (STIS_CTI), presented here as the 'CCD CTI' analysis. *Bottom:* Non-CTI corrected CCD reference image.

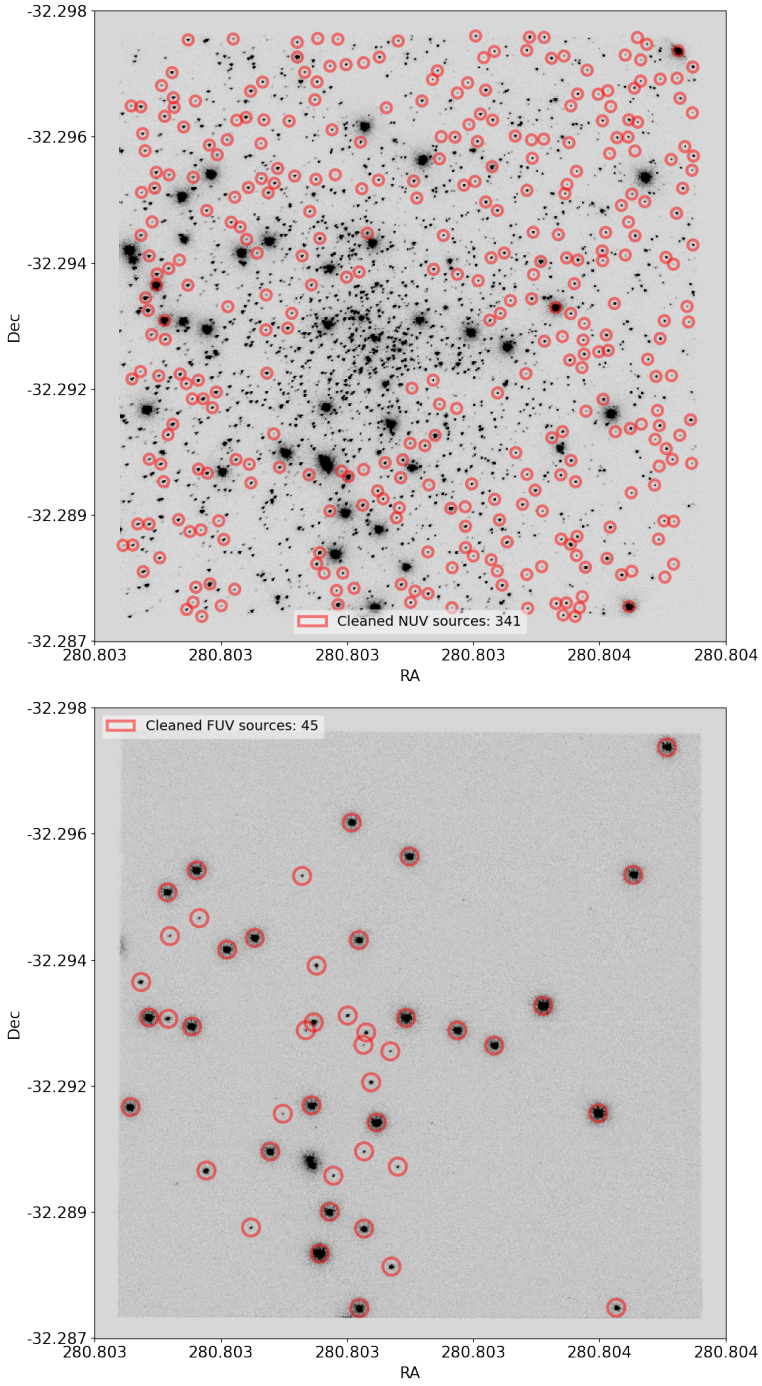

Figure 2. Cleaned list of sources (red circles) identified on the NUV (top) and FUV MAMA (bottom) reference images (obav01v9q and obav01w4q respectively) of NGC 6681. Stars with close sources (within $0.4''$), contamination, or significant asymmetry were removed from the list. Many NUV sources were not used for analysis due to overcrowding, including many of those identified in the FUV image. The FUV does not detect much of the older stellar population seen in the NUV image. *Top:* 341 NUV sources after cleaning. *Bottom:* 45 FUV sources after cleaning.

detector tailored to their image properties. These parameters determine the level of smoothing performed prior to detection (`fwhm`), threshold for a source to be detected (`threshold=10*std` used for all detectors as in ISR 2013-02), and the source properties that are used to identify round and sharp stellar objects (`roundlo`, `roundhi`, `sharphi`). We refer the reader to the PHOTUTILS.DAOSTARFINDER documentation[8] for more information on each of these parameters.

We find an initial set of 168 sources on the CCD images, as determined from the pixel-based CTI corrected CCD image. We use the same sources and positions for the non-CTI corrected CCD reference image to ensure that the trails in the non-CTI corrected images did not affect the source centering or sky background estimates. We also find an initial set of 2020 NUV sources and 52 FUV sources. We then perform some basic cleaning of the lists to identify isolated and non-contaminated stars. We remove any close pairs of sources within 0.8″ for the CCD images and within 0.4″ for the MAMAs. We then perform a final visual inspection of every source to remove any contaminated or clear non-stellar objects (not already removed by the roundness and sharpness constraints set in DAOSTARFINDER).

We identify a cleaned sample of 125 sources for the CCD, 341 for the NUV MAMA and 45 for the FUV MAMA detectors. These cleaned sources are shown on each of the reference images in Figures 1 and 2 for the CCD and MAMA detectors respectively. These numbers are close to those found in ISR 2013-02: 123 stars in the CCD, 359 stars in the NUV MAMA, and 46 stars in the FUV MAMA reference images. Comparing the different source catalogs between studies, the method presented here slightly improves the identification of brighter stars and removal of spurious sources. The FUV images of NGC 6681 show many fewer sources compared to the NUV filters as the older stellar populations of the star cluster are not bright at FUV wavelengths. The FUV bright sources are evolved blue horizontal branch stars, that could also be variable RR Lyrae stars, many of which are not in the final NUV source list after cleaning due to overcrowding.

We then identify a subset of these sources used for creating a point spread function (PSF) for each of the images. To ensure the most consistent measure of the PSF between images, we opted to use a set of stars that appeared in most, if not all, of the images. We then performed a visual inspection to identify sources with a clear profile and no signs of saturation (as determined from the reference images). We find a list of 19 stars in the CCD images, 19 stars in the NUV images and 16 stars in the FUV images that satisfy these additional constraints and are used in each image for creating its PSF.

6. PSF Creation

We use the PSFs for each image to determine appropriate aperture sizes to use for photometry. To create a PSF for each image, we stack the stars in the PSF list (clean

[8] https://photutils.readthedocs.io/en/stable/api/photutils.detection.DAOStarFinder.html

sources appearing in all/most images) using new PSF stacking tools[9]. These tools are written in Python and include simple methods for extracting, aligning and averaging PSFs in each image with flexibility for adaptation. We extract each star and interpolate them onto a sub-pixel grid for fine alignment. The PSFs are aligned on the brightest pixel and the median is taken. We interpolate the average PSF profiles back to the native pixel scale of the detectors to generate a PSF per image.

We then determine PSF full-width-half-max (FWHM) values by fitting both a 2D Moffat and Gaussian profile (using ASTROPY models[10]; Astropy Collaboration 2013, 2018) and compare the two (see Tables 4, 5, and 6 for these values). Comparing the FWHM values from the two models, we find that the Moffat FWHM values are $\sim 15\%$ smaller than the Gaussian FWHM values for the CCD and $\sim 20\%$ smaller for the MAMAs. This offset is typical between the different profile types. The median Moffat PSF FWHM value for the CCD pixel-based CTI corrected images is 1.66 pix, for the non-CTI corrected CCD is 1.74 pix, for the NUV MAMA is 2.27 pix and for the FUV MAMA is 2.07 pix. We find no significant trends of the PSF FWHM (within 1σ) with time for any of the detectors.

Generally, stellar profiles are best characterized by Moffat profiles (as used for the CCD, NUV and most of the FUV image PSFs). This breaks down for saturated FUV stars which are better approximated by Gaussian profiles. The PSF profiles are used for setting the aperture width for photometry (radii of $5\times$ PSF FWHM) so for the subset of FUV images with a PSF showing signs of saturation, we adopt a Gaussian profile. When the Moffat profile has a FWHM < 1.5 pixels, indicating a poor fit to the star, we use the Gaussian FWHM values. For the cases where these Gaussian FWHM values are not constrained (> 7 pixels, affecting $\sim 12\%$ of FUV images, all in the 25MAMA clear filter), we default to a minimum value of FWHM $= 1.5$ pixels. This workaround ensures that we can still measure aperture photometry from images that are more prone to saturation, however it also means that some sources will be saturated, resulting in outliers. We perform some sigma-clipping on individual stellar magnitude trends prior to determining our final results to reduce the effects of sources more prone to saturation to the overall trend results.

7. Photometry

To measure aperture photometry, we again use tools from the PHOTUTILS package. The aperture radius used for each image is $5\times$ PSF FWHM as used in ISR 2013-02. To determine a local sky background for every star, we define an annulus around each of them. We use an inner radius of $5\times$ PSF FWHM and thickness of 10 pixels for the CCD and NUV images. For the FUV images, we expanded this annulus to $10\times$ PSF FWHM inner radius and 15-pixel thickness to better sample the sky given the extended profiles of the FUV sources.

[9] https://github.com/mrevalski/hst_wfc3_psf_modeling
[10] http://www.astropy.org

To accurately sample the local background from the calibrated sky-subtracted images within the annulus and not the source itself or other contamination, we create a segmentation map used for masking. This mask uses a low 0.8 signal-to-noise ratio (SNR) detection threshold to ensure rigorous masking for the CCD and NUV images. We use a slightly higher 1.2 SNR threshold for the FUV images to ensure enough sky pixels. We then take a sigma-clipped median of the unmasked sky pixels ($\sigma = 2$, no. iterations $= 5$) and subtract this from the aperture pixels to perform local sky-subtracted photometry on each source. The errors on the aperture photometry are determined using the error arrays of each image that include shot noise. We perform aperture photometry with the PHOTUTILS.APERTURE_PHOTOMETRY routine that takes the image data with the local background subtracted, the aperture footprint, and the error array to generate accurate photometry and corresponding errors.

The measured fluxes in net counts (NC) are then converted to calibrated ST magnitudes[11] (m) with the following equations.

$$m = -2.5 \times \log_{10}(F) + \texttt{PHOTZPT} \tag{1}$$

where

$$F = NC \times \texttt{PHOTFLAM}/\texttt{TEXPTIME}. \tag{2}$$

This relation uses keywords from the headers of each image PHOTZPT (ST magnitude zeropoint), PHOTFLAM (inverse sensitivity in ergs/s/cm^2/Å per count/s), both populated by the PHOTCORR routine in the STIS pipeline from the IMPHTTAB reference file, and the total exposure time TEXPTIME. For the non-CTI corrected images, the CTI correction is then derived with the CTESTIS code and a Δm applied to the derived magnitudes (see Section 3 for more details).

8. Results

8.1 Overall Time Dependence

With magnitudes measured for the stars in each image, we then plot their magnitudes as a function of time. We do this separately for each detector to measure the effects of the TDS residuals in each. Any time dependence measured in the magnitudes represents a residual trend that persists after some initial TDS correction is applied in the STIS data pipeline. We analyze the residual trends for all stars that appear in three or more images. An inverse-variance weighted 1D polynomial is fitted to each star and a slope and error is determined.

Examples of these trends for individual stars are shown in Figures 3, 4 and 5 for the CCD, NUV MAMA and FUV MAMA images respectively. The pixel-based CTI data starts after SM4 (indicated by the red dashed line in the figures) while the

[11] https://www.stsci.edu/hst/instrumentation/acs/data-analysis/zeropoints

CCD data corrected with the empirical CTESTIS Δm values span the full time period of observations (25 years). The trends for the NUV and FUV MAMA detectors are first measured for the observations taken in all the three filters used in this analysis (color coded in the example plots) and separately for each filter in the next section.

As can be seen from the example residual TDS plots for the MAMA detectors in Figures 4 and 5, there are often magnitude offsets between the filters (top plots). This is expected as each filter spans a different wavelength range of the stellar spectral energy distributions. For the combined filter magnitude trends, these offsets between filters create artificial scatter that affects the derived slope. For the MAMA detectors, where multiple filters are combined to measure overall trends, we normalize the magnitudes to remove these offsets (magnitude − median filter magnitude) prior to fitting the 1D polynomial used for our final overall time dependence results.

The NUV/F25CN182 filter consistently shows large scatter and variation and is known to have calibration issues, an example of this shown in the top plot of Figure 4. We therefore remove it from the overall trend measurements of the NUV MAMA but still include it in the by-filter trends presented in Section 8.2. Examples of the trends fitted from these normalized magnitudes for each detector, and with the F25CN182 points removed for the NUV MAMA, are shown in the bottom plots of Figures 4 (NUV) and 5 (FUV). We note for comparison that the overall MAMA trend results from ISR 2013-02 are not derived from normalized magnitudes and did include the NUV/F25CN182 filter.

Stars measured during the same year and even in the same filter (as for the CCD) can show significant scatter. In the case of Figure 3, this scatter appears to increase with time which could be an indication of the reduced photometric calibration, that the star could be variable, or a combination of both. Comparing the level of scatter for an individual CCD source between this work and that shown in ISR 2013-02, the measurements are consistent implying that it is not a feature of the analysis methods presented here. Part of the variation could be due to the different orientations of the images (see Tables 4, 5 and 6 for the image position angles). Particularly for the CCD detector, variation may be introduced by the asymmetry in the L-flat, if for example, stars are falling on very different parts of the detector between images.

To investigate the scatter for individual sources in the MAMA detectors, we look at a subset of stars in our sample of the MAMA field (NGC 6681)[12] that are used as flux calibration standards[13] (Bohlin et al. 2014, 2020). Magnitude trends for these standards are consistent with showing no residual variation within errors over 15 years (as spanned by ISR 2013-02) and 25 years (up to 2022) for all filters combined. Some stronger trends are seen for individual filters, however, with such a small sample of stars it is hard to draw strong conclusions and we defer to the more statistically relevant

[12]Two NUV standards: NGC6681-10, NGC6681-11. Eight FUV standards: NGC6681-1, NGC6681-2, NGC6681-3, NGC6681-6, NGC6681-8, NGC6681-9, NGC6681-10, NGC6681-11

[13]https://www.stsci.edu/hst/instrumentation/reference-data-for-calibration-and-tools/astronomical-catalogs/calspec

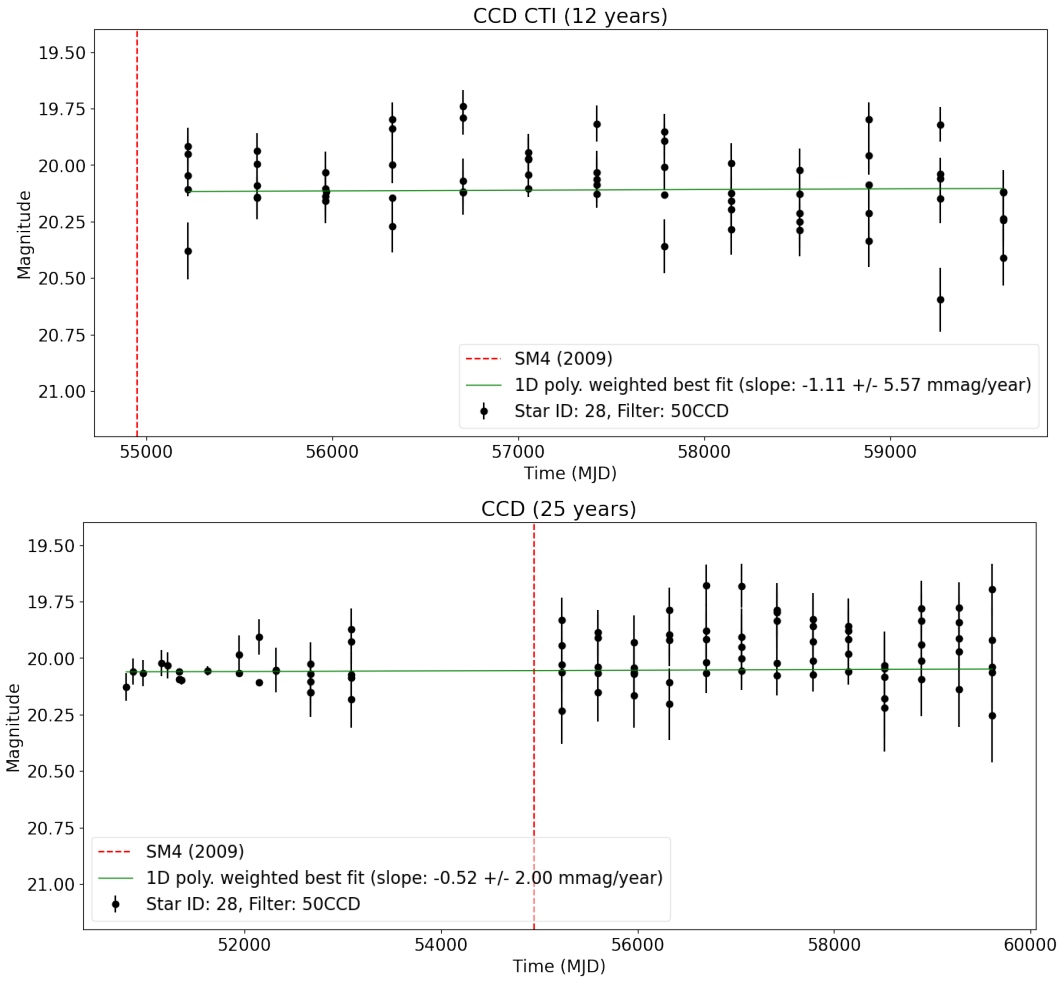

Figure 3. Example STIS CCD residual TDS trend plots (CTI corrected magnitude as a function of time) for a single star (RA=201.412128, Dec=-47.597152) in the 50CCD filter. The SM4 timestamp (red dashed line) and a weighted 1D polynomial fit to the data (green line) are shown. *Top:* Trend plot for the CCD images CTI corrected with the pixel-based STIS_CTI code (post-SM4 data only). *Bottom:* Trend plot for all available CCD data for this source with empirical CTI corrections derived with the CTESTIS code.

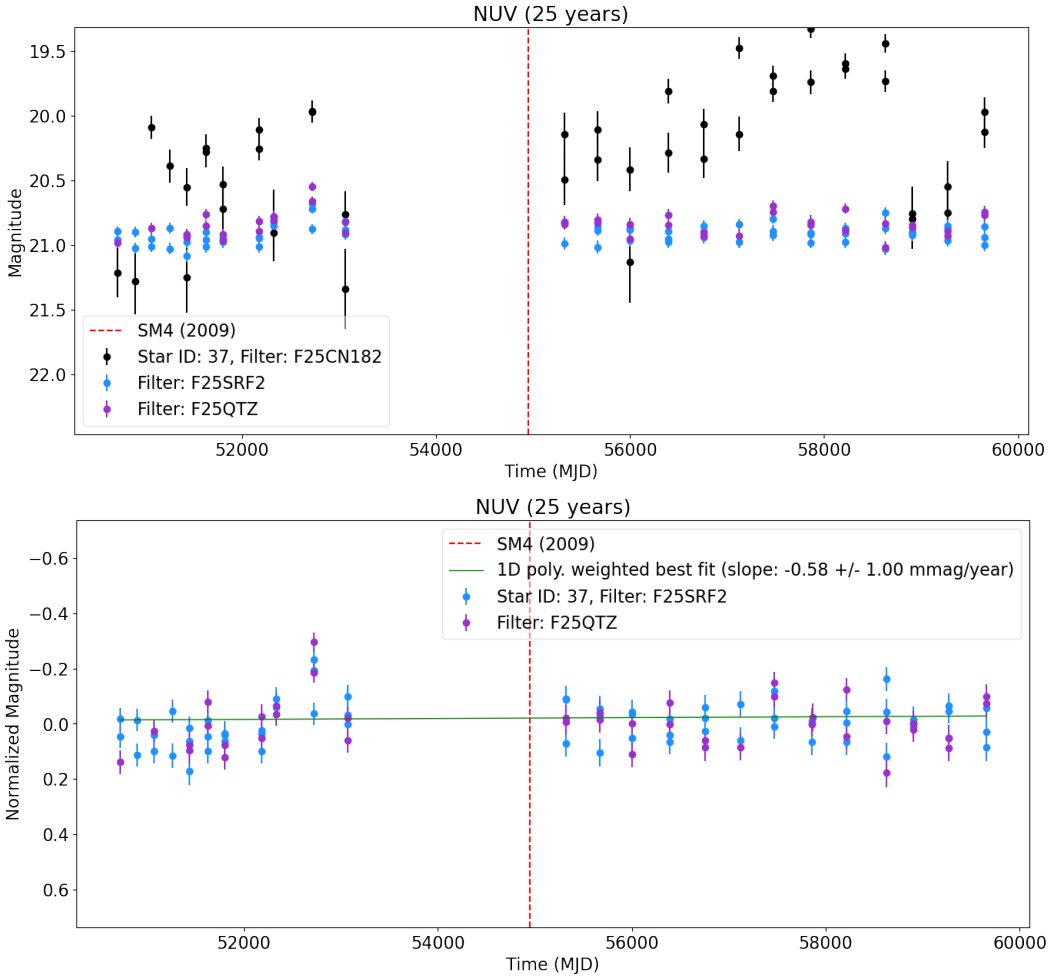

Figure 4. Example STIS NUV MAMA residual TDS trend plots (magnitude as a function of time) for a single star (RA=280.806055, Dec=-32.290307) with the same labeling as Figure 3. *Top:* NUV data shown in three filters: F25CN182 (black), F25SRF2 (blue), F25QTZ (purple). *Bottom:* Normalized magnitudes (magnitude − median filter magnitude) used for the overall MAMA trend results. Only two filters are shown (F25SRF2 and F25QTZ) as the F25CN182 filter was removed from the overall NUV MAMA detector trends due to its calibration issues.

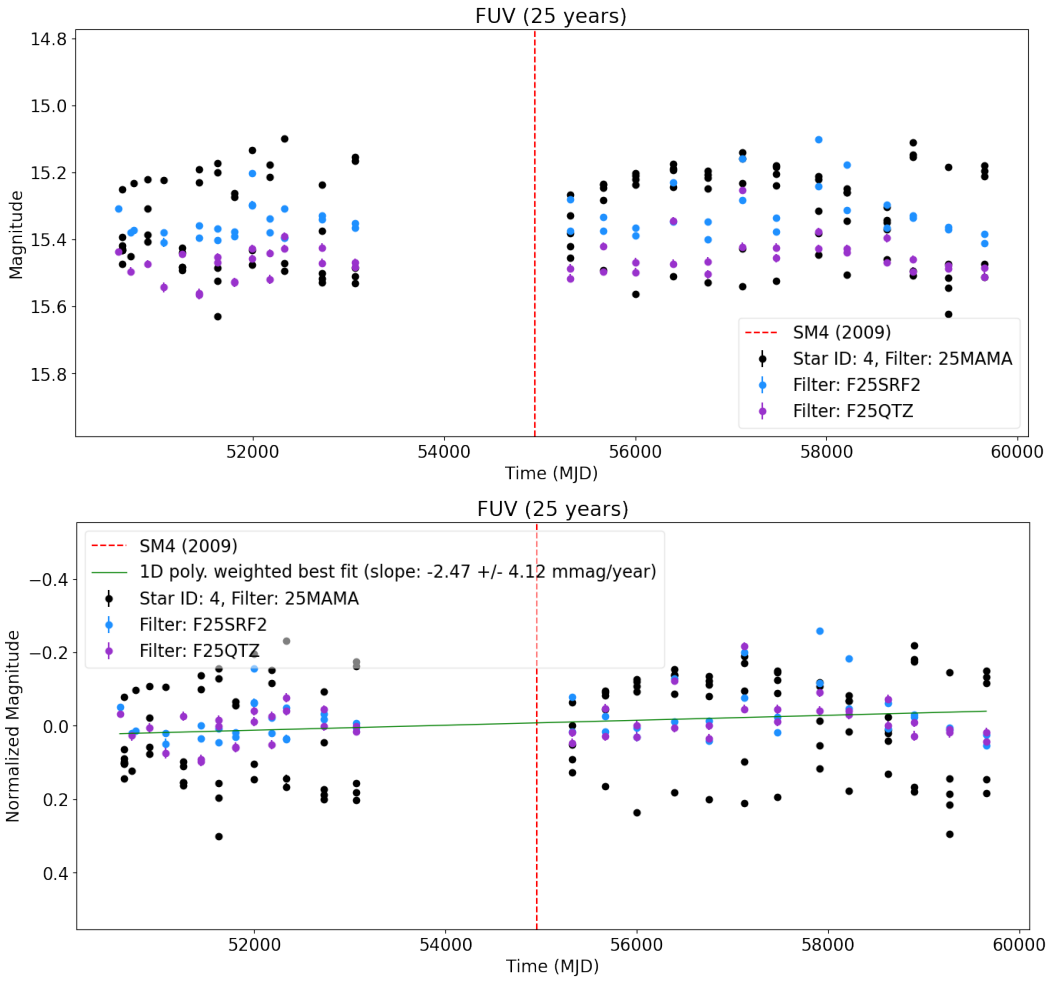

Figure 5. Example STIS FUV MAMA residual TDS trend plots (magnitude as a function of time) for a single star (RA=280.804551, Dec=-32.289792) with the same labeling as Figure 3. *Top:* FUV data shown in three filters: 25MAMA (black), F25SRF2 (blue), F25QTZ (purple). *Bottom:* Normalized magnitudes (magnitude − median filter magnitude) used for the overall MAMA trend results.

Table 1. Results summary of the full-field sensitivity analysis and TDS residual trends by detector/type, study, and time period. All filters are included for the ISR 2013-02, CCD and FUV results. NUV overall trend results for this work include only the F25SRF2 and F25QTZ filters. The MAMA trends for this work include normalization between filters before slopes are fitted to remove the filter offsets.

Analysis	Detector	Number of Years	Final Number of Stars	% Clipped from Total	Weighted Mean Slope (mmag/year)	Standard Deviation (mmag/year)	% Flux Change Over Years
ISR 2013-02	CCD	15	106	-	0.50 ± 0.06	15.80	-0.69
(1997–2012)	NUV	15	344	-	-0.04 ± 0.02	4.19	0.06
	FUV	15	46	-	0.54 ± 0.04	3.74	-0.74
This Work	CCD	15	108	13.6	0.34 ± 0.24	7.30	-0.47
(1997–2012)	NUV	15	326	4.4	-0.39 ± 0.13	6.55	0.54
	FUV	15	39	13.3	-0.41 ± 0.40	3.19	0.57
This Work	CCD CTI	12	110	12.0	-0.21 ± 0.23	5.56	0.23
(All Years)	CCD	25	107	14.4	-0.60 ± 0.13	5.23	1.38
	NUV	25	315	7.6	-0.25 ± 0.05	3.09	0.56
	FUV	25	36	20.0	-1.56 ± 0.18	2.17	3.53

overall trends present here.

We 3σ-clip the distribution of derived slopes to remove any poorly fitted or unconstrained slopes (driven in part by saturated sources in some images, mostly affecting the FUV). We determine statistics of the sigma-clipped distributions, median, weighted mean and associated error, and standard deviations in mmag/year to derive our final results. Histograms of the clipped slope distributions and some basic statistics are shown in Figures 6 and 7 for the CCD and MAMA results respectively. As we present the weighted mean as our main result, we adopt the standard error for the weighted mean for the associated errors rather than the regular standard error on the mean ($\sigma/\sqrt{n}$). The histograms in Figures 6 and 7 do show considerable scatter that could be driven by calibration or instrumental effects, or intrinsic variation from variable stars. However, the inverse-variance weighted averages include the uncertainty and scatter of the individual slope measurements that is not captured from the histograms or a simple standard deviation.

We determine a percentage flux change from the weighted mean slope values using the fractional form of the magnitude-to-flux relation. A negative magnitude slope corresponds to a star appearing brighter with time, and therefore a positive percentage flux change. We have corrected this sign change relative to ISR 2013-02 in this work and for the ISR 2013-02 results presented in Tables 1, 2, and 3, to allow for a direct comparison. We present a summary of the overall trend results from this work and a comparison to the results of the previous analysis in ISR 2013-02 in Table 1. The top

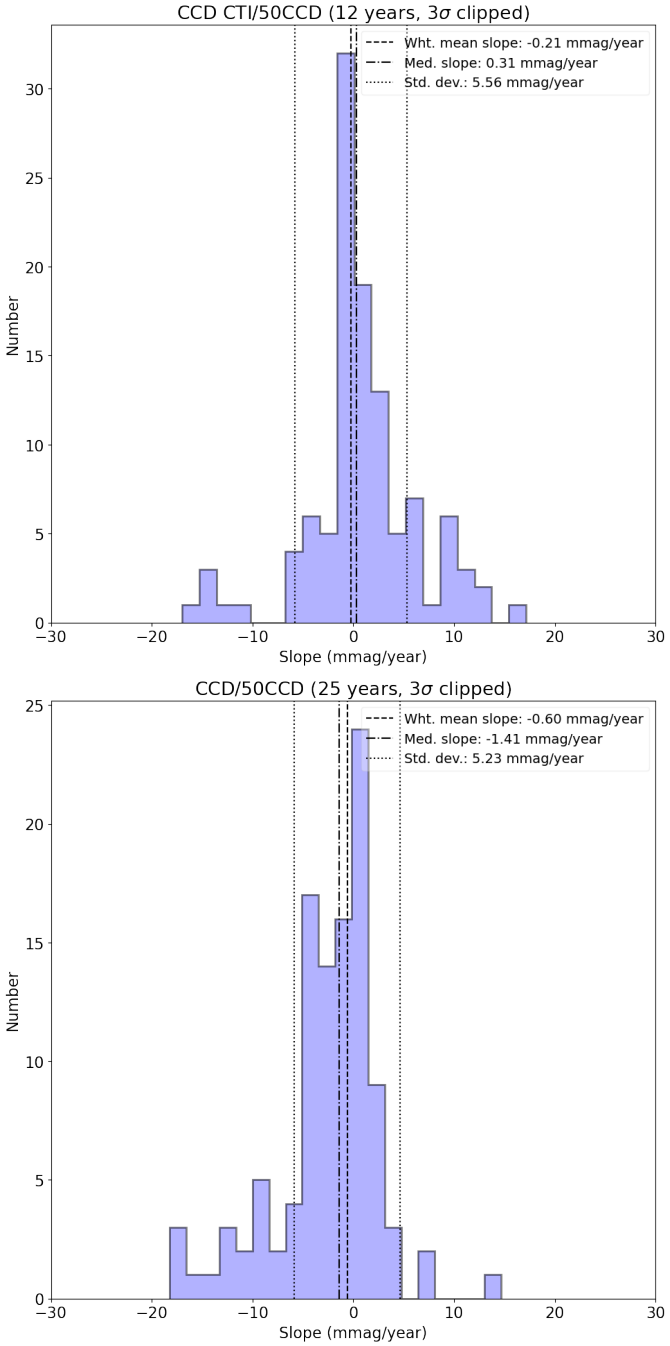

Figure 6. Sigma-clipped histograms of slopes derived from weighted 1D polynomial fits to the CCD data (50CCD filter). The data have been 3σ-clipped to remove extreme outliers (i.e., poorly fitted stars), see Table 1 for a summary. The weighted mean (black dashed line), median (dot-dashed line), and standard deviation (dotted lines) of the clipped slope distribution are shown. *Top:* Slope distribution for the post-SM4 CCD data (spanning 12 years) CTI corrected with the pixel-based code (STIS_CTI). *Bottom:* Slope distribution for all CCD data (spanning 25 years). CTI corrections derived with the empirical CTESTIS code.

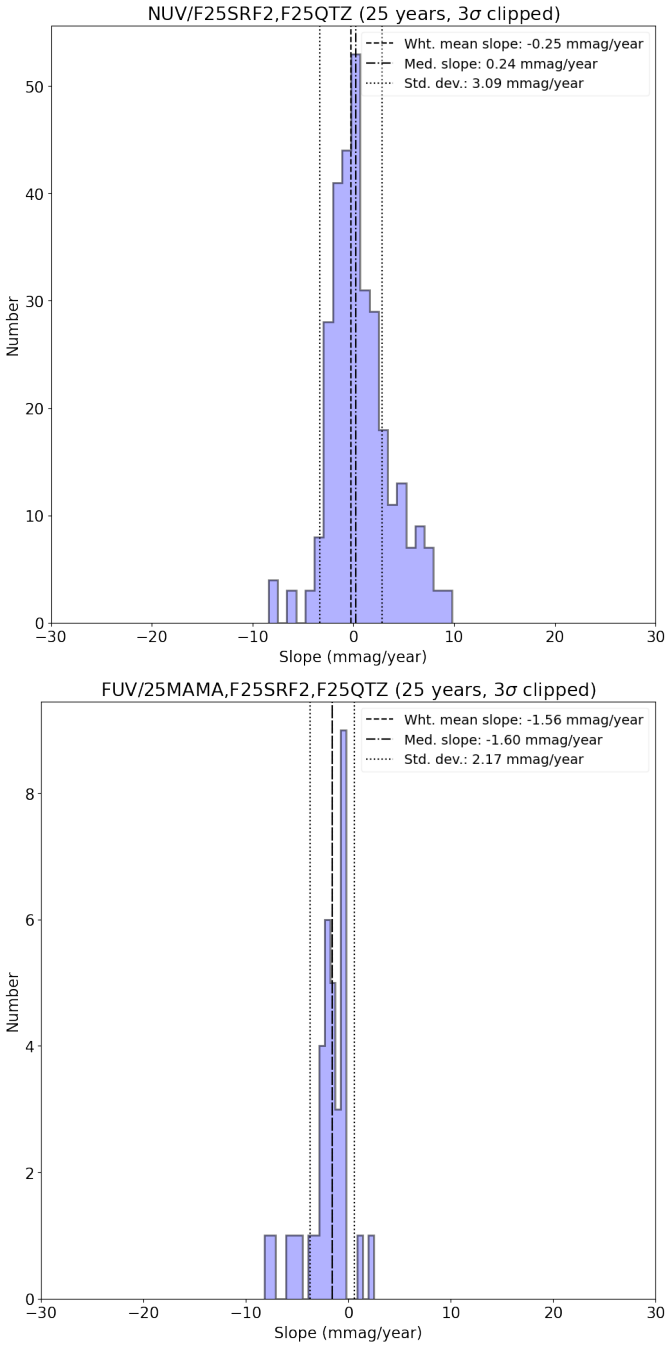

Figure 7. Sigma-clipped histograms of slopes derived from weighted 1D polynomial fits to the MAMA magnitudes normalized between filters (spanning 25 years). The plots have the same labeling as Figure 6. The data have been 3σ-clipped to remove extreme outliers (i.e., poorly fitted stars), see Table 1 for a summary. *Top:* NUV MAMA slopes measured from normalized magnitudes in two filters (F25SRF2, F25QTZ), F25CN182 was removed due to calibration issues. *Bottom:* FUV MAMA slopes measured from normalized magnitudes in all three filters (25MAMA, F25SRF2, F25QTZ).

rows show the overall trend results from ISR 2013-02, we then show the results from this work spanning the same time period as ISR 2013-02 (1997 to 2012), and the final rows show the results from this work for all years available (up to 2022) split by detector. We show the final number of stars used in the analysis (after sigma-clipping), and for this study, the percentage of individual star slopes sigma-clipped to determine the final statistics (between $\sim$ 4–20%) for each study and time period.

There are some discrepancies between the results from this work and the previous analysis spanning the same time period. This is to be expected to some degree given the differences in codes and photometry methods used in the analysis and using normalized magnitudes for the MAMAs. Where possible, methods were developed in Python to closely match those used in the previous study (that used IDL). Additionally, since the previous analysis there have been updates to the STIS calibration pipeline and reference files (e.g., FUV distortion), which also contribute to the discrepancies. Generally though, the residual TDS trends for the three detectors as measured up to 2012 are within the 1% quoted absolute flux calibration accuracy for STIS over 15 years. ISR 2013-02 concluded that no additional calibrations were required at that time but that monitoring should continue. As done in ISR 2013-02, we also investigate the correlation between slope and magnitude and find no significant trends.

When extending the FFSM analysis to 2022, the measured residual magnitude trend slopes for the CCD show a reversal from positive to negative. Despite the trend reversal, the CCD trends remain close to the 1% STIS flux accuracy (1.38%). The CCD CTI results include only pixel-based CTI corrected data from post SM4 and show much smaller residual trends but they are in line with the negative magnitude trends seen in all the CCD data.

The FUV MAMA results show a stronger trend when including data up to 2022, beyond the 1% quoted flux calibration accuracy (3.53%). As demonstrated in Section 8.2, this trend is mostly driven by the FUV/25MAMA filter. This shift may be driven in part by the release of a new Image Photometry Table (IMPHTTAB)[14] which improves the photometric calibration, and impacts data taken after 2014 most significantly (i.e., after the last prior IMPHTTAB release) as the calibration previously relied on extrapolated values past that date. The TDS models may also be contributing to these trends, especially for the FUV MAMA that is subject to increased scatter (up to $\sim$ 4%) for post SM4 data (e.g., ISR 2017-06). The NUV MAMA trends when not including the F25CN182 filter show no change in trend within errors. Percentage flux change values for the NUV MAMA with normalization and the F25CN182 filter included would be -1.4% up to 2012 and -0.93% up to 2022. We discuss possible additional physical drivers of these results in Section 9.

[14] Announced in STIS STAN October 2021.

Table 2. Results summary of the NUV MAMA full-field sensitivity analysis and TDS residual trends by filter, study, and time period.

Analysis	Detector & Filter	Number of Years	Final Number of Stars	% Clipped from Total	Weighted Mean Slope (mmag/year)	Standard Deviation (mmag/year)	% Flux Change Over Years
ISR 2013-02 (1997–2012)	NUV/F25SRF2	15	340	-	0.18 ± 0.03	4.49	-0.25
	NUV/F25QTZ	15	330	-	0.04 ± 0.05	7.29	-0.05
	NUV/F25CN182	15	290	-	0.88 ± 0.13	18.90	-1.22
This Work (1997–2012)	NUV/F25SRF2	15	326	4.4	-0.83 ± 0.14	7.06	1.14
	NUV/F25QTZ	15	324	5.0	0.70 ± 0.21	8.45	-0.97
	NUV/F25CN182	15	337	1.2	-5.36 ± 0.63	23.79	7.13
This Work (All Years)	NUV/F25SRF2	25	322	5.6	-0.61 ± 0.06	3.13	1.39
	NUV/F25QTZ	25	311	8.8	0.35 ± 0.09	4.83	-0.80
	NUV/F25CN182	25	341	0.0	-2.36 ± 0.27	15.60	5.30

8.2 Filter Dependence for MAMAs

We also measure the TDS residuals by filter for the NUV and FUV MAMA detectors. The summary of these trends is shown Tables 2 and 3 for the NUV and FUV filters respectively. As before, we show the results split by study (STIS ISR 2013-02 and this analysis) and time period (1997–2012 and 1997–2022) to aid with direct comparison. The magnitudes measured for the individual filters do not require normalization. However, there is significant scatter and variation seen in the F25CN182 filter and fewer data points, so trends measured from that filter are less reliable. The quartz filters (F25QTZ) show more stability with time relative to the other filters which may be more subject accumulating defects (e.g., pinholes). These effects were measured in the WFPC2 instrument filters after 16 years on orbit (WFPC2 ISR 2010-05, Lim et al. 2010).

We again see some discrepancies between the two studies spanning the same time period, which are probably driven by the previously discussed data and analysis differences. For the NUV filters, the residual trends are most pronounced for the F25CN182 filter for both time periods (1997–2012 and 1997–2022). The FUV filters are more consistent to each other but each show significant trends, stronger than the $\sim 2\%$ found in ISR 2013-02. A move to reduced and stronger negative magnitude residual TDS trends is seen in all FUV filters when including the more recent data. As shown in the image summary Tables 5 and 6 for the NUV and FUV MAMA detectors respectively, the NUV/F25SRF2 and FUV/25MAMA observations are far more numerous. This could make these filters more statistically reliable than the other filters alone for tracking accurate trends. However, the FUV/25MAMA filter is more prone to saturation which decreases it reliability.

Table 3. Results summary of the FUV MAMA full-field sensitivity analysis and TDS residual trends by filter, study, and time period.

Analysis	Detector & Filter	Number of Years	Final Number of Stars	% Clipped from Total	Weighted Mean Slope (mmag/year)	Standard Deviation (mmag/year)	% Flux Change Over Years
ISR 2013-02	FUV/F25SRF2	15	46	-	1.39 ± 0.08	3.70	-1.92
(1997–2012)	FUV/F25QTZ	15	46	-	-0.36 ± 0.12	3.20	0.50
	FUV/25MAMA	15	45	-	1.25 ± 0.05	3.60	-1.73
This Work	FUV/F25SRF2	15	37	17.8	3.28 ± 0.38	3.37	-4.64
(1997–2012)	FUV/F25QTZ	15	42	6.7	2.37 ± 0.33	3.94	-3.33
	FUV/25MAMA	15	43	4.4	-1.96 ± 0.68	3.47	2.67
This Work	FUV/F25SRF2	25	37	17.8	-0.47 ± 0.23	3.82	1.07
(All Years)	FUV/F25QTZ	25	38	15.6	0.45 ± 0.18	2.90	-1.03
	FUV/25MAMA	25	41	8.9	-2.58 ± 0.30	1.91	5.77

9. Discussion & Conclusions

In this analysis, we look at the full-field sensitivity of the three detectors on STIS. STIS imaging data go through an initial TDS correction in the CALSTIS pipeline based on calibrations derived from spectroscopic data. The goal of this analysis is to measure if there are any residual trends after these corrections are applied to see how well they are performing. This study builds off the previous analysis performed 10 years ago (up to 2012) presented in STIS ISR 2013-02. We develop analogous analysis methods in Python to the IDL routines previously used.

We first determine PSFs for each image, and find no significant trends of the PSF FWHM with time for any of the detectors. We then measure aperture photometry on a sample of clean isolated sources identified in CCD images (of NGC 5139) and NUV and FUV MAMA images (of NGC 6681). We track the residual magnitude trends of each star with time by determining weighted 1D polynomial fits to derive their slopes. For the MAMA detectors, we perform normalization of the magnitudes between the filters used in the overall trends prior to fitting slopes. We determine the overall (for all detectors) and filter dependent (for the MAMAs) residual trends by calculating sigma-clipped statistics and compare these results with the previous analysis and how these have evolved over the last ten years.

We find some discrepancy between the results in this work and that of ISR 2013-02 over the same time period. These can likely be explained by the differences in the analysis methods, codes and updated STIS pipeline calibrations applied between studies. Generally, we find the overall trends are within the quoted 1% STIS flux calibration accuracy. Only the FUV MAMA overall trend up to 2022 deviates from these errors with a percentage flux change of 3.53%, which is largely driven by the

25MAMA filter.

For the individual filter trends for the MAMAs, we find that up to 2022 the uncertainties remain close to the 1% flux calibration accuracy for STIS for all filters but the NUV/F25CN182 (removed from the overall NUV MAMA trends due to calibration issues) and FUV/25MAMA. The larger NUV and FUV MAMA residual trends for these filters are on the order of the TDS corrections themselves ($\sim 5\%$, see Tables 2 and 3 for NUV and FUV respectively). These results could imply that the imaging sensitivity in these MAMA filters may have only decreased by 5% compared with the 10–15% TDS changes predicted from spectroscopic analysis. However, there are also fewer observations in the separate MAMA filters, making it harder to reliably model and track their trends over time. The FUV MAMA filters show a wider variation in the post-SM4 data (~ 2.5–5%), perhaps influenced by the increased scatter in the TDS measured in post SM4 data (e.g., ISR 2017-06). FUV/25MAMA remains an outlier in the results up to 2022 which could be driven by these TDS uncertainties or because this filter is more subject to saturation. It could also be more sensitive to FUV-bright variable stars, such as RR Lyraes, that can have large magnitude variations (~ 0.5–1 mag).

The more significant result seen for all detectors are stronger negative magnitude trends when including the data from the last ~ 10 years. These residual trends result in the same star appearing brighter with time (negative magnitude trend corresponds to positive percentage flux change). A detector loses sensitivity with time, so models are used to correct for this and scale stellar fluxes back up to their true value. This increase in stellar brightness following the TDS correction implies that the current TDS models are over correcting the fluxes, an effect that appears to be increasing with time. These results may mean that there is a slowdown in the detector sensitivity loss which also seems to be present in WFC3/UVIS standard star observations in a few filters and additionally measured in ACS and COS. Some sensitivity loss slowdown with time is expected due to the degradation of the detectors, however, this is considered with the spectroscopic STIS TDS models (e.g., ISR 2017-06). Measurements of the residual trends for STIS imaging shows that the sensitivity loss may be slowing more rapidly than expected relative to the spectroscopically calibrated TDS models.

10. Recommendations

The overall residual TDS trends determined in this analysis of STIS imaging data up to 2022 are mostly consistent with the $\sim 1\%$ the quoted flux calibration accuracy for STIS. These errors do not hold for the NUV/F25CN182 (that was excluded from the overall NUV MAMA trends) or FUV/25MAMA filters. We recommend that users adopt the values presented in Table 1 as the most accurate measure of the residual TDS trends for each detector. The increased uncertainties for the NUV/F25CN182 and FUV/25MAMA filters should be noted for users wishing to use these apertures to ensure they can plan adequately for more accurate flux calibrations if required. An investigation into how orientation affects the variation of different measurements could also be of interest in

future. Additionally, identifying which stars are classified as RR Lyrae variables could provide insights into which stars are increasing scatter in the MAMA detectors.

The generalized TDS models applied to correct the STIS imaging data for each detector were trained on spectroscopic data. This analysis has highlighted that revisiting these assumed TDS models for some of the outlier filters could be valuable to reduce the residuals and uncertainties in STIS imaging data. This is most important for data taken after SM4, and particularly data observed in the last few years where a slowdown in sensitivity loss may be occurring faster for STIS imaging than spectroscopic data. TDS trends measured directly from imaging would likely improve their calibration, rather than relying on spectroscopic calibrations alone. We recommend that the monitoring of these star fields continue for all detectors to ensure we can accurately track their TDS trends with time.

Acknowledgments

Thanks to Svea Hernandez, Annalisa Calamida and Joleen Carlberg for reviewing this ISR and providing valuable insights to strengthen the analysis. Thanks also to the STIS team for useful discussions that helped shape the analysis presented here. Thanks to Sean Lockwood and Paul Goudfrooij for helpful advice on implementing the CCD CTI corrections. Thanks also to Julia Roman-Duval for answering questions on the analysis presented in ISR 2013-02.

This research is based on observations made with the NASA/ESA *Hubble Space Telescope* obtained from the Space Telescope Science Institute. All of the data presented in this ISR were obtained from the Mikulski Archive for Space Telescopes (MAST). STScI is operated by the Association of Universities for Research in Astronomy, Inc., under NASA contract NAS5-26555.

References

Anderson, J., & Bedin, L. R., 2010, PASP, 122, 895
Astropy Collaboration et al., 2013, A&A 558, A33
Astropy Collaboration et al., 2018, arXiv:1801.02634
Bohlin, R. C., Gordon, K. D., & Tremblay, P.-E. 2014, PASP, 126, 711
Bohlin, R. C., Deustua, S. E., & de Rosa, G., 2019, AJ, 158, 5
Biretta, J., Lockwood, S., & Debes J., 2015, STIS Instrument Science Report 2015-04
Bohlin, R. C., Hubeny, I., & Rauch, T., 2020, AJ, 160, 21
Bradley et al., 2020, Zenodo, astropy/photutils: 1.0.2
Carlberg, J. K., & Monroe, T., 2017, STIS Instrument Science Report 2017-06
Ginsburg, A., Sipocz, B. M., & Brasseur, C. E., et al., 2019, AJ, 157, 98
Gonzaga, S., Hack, W., Fruchter, A., & Mack, J. 2012, The DrizzlePac Handbook (Baltimore, MD: STScI)
Goudfrooij, P., & Bohlin, R., 2006, STIS Instrument Science Report 2006-03
Goudfrooij, P., Bohlin, R. C., Maíz-Apellániz, J., & Kimble, R. A., 2006, PASP, 118,

848
Hoffmann, S. L., Mack, J., et al., 2021, The DrizzlePac Handbook, Version 2.0 (Baltimore: STScI)
Lim, P. L., Quijada, M., Baggett, S., Biretta, J., MacKenty, J., Boucarut, R., Rice, S., & del Hoyo, J., WFPC2 Instrument Science Report 2010-05
Prichard, L., STIS Instrument Science Report 2022-03
Prichard, L., Welty, D. and Jones, A., et al. 2022 "STIS Instrument Handbook," Version 21.0, (Baltimore: STScI)
Roman-Duval, J., & Proffitt, C., 2013, STIS Instrument Science Report 2013-02
Sohn, S. T., 2018, STIS Instrument Science Report 2018-02
Stys, D. J., Bohlin, R., C., & Goudfrooij, P., 2004, STIS Instrument Science Report 2004-04

Appendix A

Table 4. STIS CCD exposures used in this analysis and their properties. The reference image is indicated with a † symbol. Post-SM4 exposures also CTI corrected with the pixel-based code (STIS_CTI) for comparison and presented as the 'CCD CTI' analysis indicated with '*'s and their PSF FWHMs given in parentheses.

Exposure	Program ID	Date of Observation	Exposure Time (s)	Aperture	Orientation (PA_APER)	PSF FWHM (Moffat, pix)	PSF FWHM (Gauss, pix)
o3zf01010	7079	1997-05-24	60.0	50CCD	7.66	1.85	2.23
o3zf01020	7079	1997-05-24	60.0	50CCD	7.66	1.85	2.21
o3zf01030	7079	1997-05-24	60.0	50CCD	7.66	1.87	2.19
o3zf01040	7079	1997-05-24	60.0	50CCD	7.66	1.99	2.30
o3zf01090	7079	1997-05-24	64.0	50CCD	7.66	1.97	2.23
o3zf010a0	7079	1997-05-24	72.0	50CCD	7.66	1.93	2.22
o3zf010b0	7079	1997-05-24	72.0	50CCD	7.66	1.83	2.22
o3zf010c0	7079	1997-05-24	72.0	50CCD	7.66	1.75	2.11
o3zf010d0	7079	1997-05-24	72.0	50CCD	7.66	2.03	2.36
o3zf010e0	7079	1997-05-24	72.0	50CCD	7.66	1.89	2.26
o3zf010f0	7079	1997-05-24	72.0	50CCD	7.66	1.79	2.09
o3zf010g0	7079	1997-05-24	72.0	50CCD	7.66	1.74	2.02
o4go02010	7639	1997-12-16	15.0	50CCD	-136.98	1.80	2.05
o4go03010	7639	1998-02-26	15.0	50CCD	-101.31	1.80	2.00
o4go04010	7639	1998-06-01	15.0	50CCD	38.02	1.78	2.02
o4go05010	7639	1998-12-10	15.0	50CCD	-145.58	1.84	2.22
o4go01010	7639	1999-02-07	15.0	50CCD	-102.71	1.77	2.04
o52301020	8056	1999-06-04	480.0	50CCD	36.05	1.89	2.16
o52301030	8056	1999-06-04	90.0	50CCD	36.05	1.80	2.06
o5ir01010	8416	1999-07-02	50.0	50CCD	45.02	1.76	2.02
o5ir02010	8416	2000-03-26	50.0	50CCD	-49.98	1.85	2.08
o69902010	8847	2001-02-03	10.0	50CCD	-94.98	1.69	2.02
o69902020	8847	2001-02-03	60.0	50CCD	-94.98	1.73	2.06
o6ib01010	8912	2001-09-01	10.0	50CCD	89.84	1.76	2.06
o6ib01020	8912	2001-09-01	60.0	50CCD	89.84	1.73	2.00
o6ib02010	8912	2002-02-15	10.0	50CCD	-94.98	1.76	2.06
o6ib02020	8912	2002-02-15	60.0	50CCD	-94.98	1.70	2.01
o8h701010	9622	2003-02-05	10.0	50CCD	-94.98	1.71	2.00
o8h701020	9622	2003-02-05	10.0	50CCD	-94.98	1.66	1.89
o8h701030	9622	2003-02-05	10.0	50CCD	-94.98	1.76	1.99
o8h701040	9622	2003-02-05	10.0	50CCD	-94.98	1.67	1.91
o8h701050	9622	2003-02-05	60.0	50CCD	-94.98	1.71	1.98
o8uv01010	10028	2004-03-20	10.0	50CCD	-72.90	1.75	2.01
o8uv01020	10028	2004-03-20	10.0	50CCD	-72.90	1.75	1.99
o8uv01030	10028	2004-03-20	10.0	50CCD	-72.91	1.82	2.08
o8uv01040	10028	2004-03-20	10.0	50CCD	-72.90	1.79	2.03
o8uv01050	10028	2004-03-20	60.0	50CCD	-72.90	1.79	2.05
obat01010*	11854	2010-01-30	10.0	50CCD	-94.98	1.71 (1.69)	2.15 (2.06)
obat01020*	11854	2010-01-30	10.0	50CCD	-94.98	1.69 (1.65)	2.07 (1.98)
obat01030*	11854	2010-01-30	10.0	50CCD	-94.98	1.68 (1.66)	1.97 (1.95)
obat01040*	11854	2010-01-30	10.0	50CCD	-94.98	1.66 (1.62)	1.93 (1.87)
obat01050*†	11854	2010-01-30	60.0	50CCD	-94.98	1.70 (1.69)	2.01 (1.99)

Table 4. (cont'd)

Exposure	Program ID	Date of Observation	Exposure Time (s)	Aperture	Orientation (PA_APER)	PSF FWHM (Moffat, pix)	PSF FWHM (Gauss, pix)
obmj01010*	12409	2011-02-05	10.0	50CCD	-94.98	1.57 (1.55)	1.83 (1.80)
obmj01020*	12409	2011-02-05	10.0	50CCD	-94.98	1.59 (1.59)	1.83 (1.82)
obmj01030*	12409	2011-02-05	10.0	50CCD	-94.98	1.61 (1.59)	1.84 (1.82)
obmj01040*	12409	2011-02-05	10.0	50CCD	-94.98	1.54 (1.54)	1.78 (1.77)
obmj01050*	12409	2011-02-05	60.0	50CCD	-94.98	1.70 (1.69)	1.97 (1.95)
obuo01010*	12770	2012-02-09	10.0	50CCD	-94.98	1.65 (1.62)	1.91 (1.85)
obuo01020*	12770	2012-02-09	10.0	50CCD	-94.98	1.60 (1.61)	1.88 (1.85)
obuo01030*	12770	2012-02-09	10.0	50CCD	-94.98	1.69 (1.65)	1.95 (1.88)
obuo01040*	12770	2012-02-09	10.0	50CCD	-94.98	1.74 (1.69)	1.93 (1.88)
obuo01050*	12770	2012-02-10	60.0	50CCD	-94.98	1.72 (1.71)	1.97 (1.95)
oc5401010*	13139	2013-01-31	10.0	50CCD	-94.98	1.68 (1.65)	1.94 (1.91)
oc5401020*	13139	2013-01-31	10.0	50CCD	-94.98	1.69 (1.61)	1.95 (1.89)
oc5401030*	13139	2013-01-31	10.0	50CCD	-94.98	1.68 (1.66)	1.92 (1.90)
oc5401040*	13139	2013-01-31	10.0	50CCD	-94.98	1.72 (1.72)	1.96 (1.97)
oc5401050*	13139	2013-01-31	60.0	50CCD	-94.98	1.74 (1.71)	1.98 (1.96)
ocfg01010*	13542	2014-02-15	10.0	50CCD	-94.98	1.73 (1.69)	2.06 (1.99)
ocfg01020*	13542	2014-02-15	10.0	50CCD	-94.98	1.77 (1.66)	2.16 (1.99)
ocfg01030*	13542	2014-02-15	10.0	50CCD	-94.98	1.78 (1.75)	2.07 (2.02)
ocfg01040*	13542	2014-02-15	10.0	50CCD	-94.98	1.67 (1.65)	2.01 (1.98)
ocfg01050*	13542	2014-02-15	60.0	50CCD	-94.98	1.74 (1.74)	2.04 (2.02)
ocrj01010*	13989	2015-02-04	10.0	50CCD	-94.98	1.88 (1.82)	2.25 (2.16)
ocrj01020*	13989	2015-02-04	10.0	50CCD	-94.98	1.71 (1.64)	2.07 (1.94)
ocrj01030*	13989	2015-02-04	10.0	50CCD	-94.98	1.74 (1.72)	2.04 (2.01)
ocrj01040*	13989	2015-02-04	10.0	50CCD	-94.98	1.75 (1.72)	2.02 (1.94)
ocrj01050*	13989	2015-02-04	60.0	50CCD	-94.98	1.83 (1.81)	2.13 (2.09)
od1r31010*	14421	2016-02-03	10.0	50CCD	-94.98	1.82 (1.77)	2.43 (2.25)
od1r31020*	14421	2016-02-03	10.0	50CCD	-94.98	1.74 (1.69)	2.30 (2.15)
od1r31030*	14421	2016-02-03	10.0	50CCD	-94.98	1.82 (1.79)	2.33 (2.22)
od1r31040*	14421	2016-02-03	10.0	50CCD	-94.98	1.76 (1.72)	2.23 (2.14)
od1r31050*	14421	2016-02-03	60.0	50CCD	-94.98	1.75 (1.75)	2.15 (2.12)
odbc01010*	14827	2017-02-02	10.0	50CCD	-94.98	1.69 (1.63)	2.06 (1.97)
odbc01020*	14827	2017-02-02	10.0	50CCD	-94.98	1.54 (1.47)	2.00 (1.85)
odbc01030*	14827	2017-02-02	10.0	50CCD	-94.98	1.69 (1.59)	2.06 (1.92)
odbc01040*	14827	2017-02-02	10.0	50CCD	-94.98	1.63 (1.57)	1.99 (1.90)
odbc01050*	14827	2017-02-03	60.0	50CCD	-94.98	1.72 (1.67)	2.11 (2.02)
odpf01010*	14968	2018-01-30	10.0	50CCD	-94.98	1.77 (1.67)	2.34 (2.12)
odpf01020*	14968	2018-01-30	10.0	50CCD	-94.98	1.68 (1.57)	2.00 (1.84)
odpf01030*	14968	2018-01-30	10.0	50CCD	-94.98	1.61 (1.60)	1.98 (1.90)
odpf01040*	14968	2018-01-30	10.0	50CCD	-94.98	1.71 (1.69)	2.07 (1.99)
odpf01050*	14968	2018-01-30	60.0	50CCD	-94.98	1.73 (1.68)	2.05 (1.97)
odw401010*	15556	2019-02-01	8.8	50CCD	-94.98	1.58 (1.55)	1.88 (1.83)
odw401020*	15556	2019-02-01	10.0	50CCD	-94.98	1.70 (1.68)	2.06 (1.99)

Table 4. (cont'd)

Exposure	Program ID	Date of Observation	Exposure Time (s)	Aperture	Orientation (PA_APER)	PSF FWHM (Moffat, pix)	PSF FWHM (Gauss, pix)
odw401030*	15556	2019-02-01	10.0	50CCD	-94.98	1.71 (1.70)	2.16 (2.05)
odw401040*	15556	2019-02-01	10.0	50CCD	-94.98	1.77 (1.63)	2.22 (1.98)
odw401050*	15556	2019-02-01	60.0	50CCD	-94.98	1.74 (1.69)	2.10 (2.02)
oe6801010*	15745	2020-02-08	60.0	50CCD	-94.98	1.86 (1.81)	2.19 (2.13)
oe6801020*	15745	2020-02-08	10.0	50CCD	-94.98	1.67 (1.58)	2.01 (1.86)
oe6801030*	15745	2020-02-08	10.0	50CCD	-94.98	1.65 (1.57)	2.05 (1.88)
oe6801040*	15745	2020-02-08	10.0	50CCD	-94.98	1.76 (1.66)	1.99 (1.89)
oe6801050*	15745	2020-02-08	10.0	50CCD	-94.98	1.68 (1.62)	1.97 (1.87)
oeef01010*	16347	2021-02-24	60.0	50CCD	-94.98	1.77 (1.78)	2.16 (2.10)
oeef01020*	16347	2021-02-24	10.0	50CCD	-94.98	1.58 (1.64)	1.98 (1.96)
oeef01030*	16347	2021-02-24	10.0	50CCD	-94.98	1.55 (1.59)	1.95 (1.90)
oeef01040*	16347	2021-02-24	10.0	50CCD	-94.98	1.74 (1.72)	2.06 (1.99)
oeef01050*	16347	2021-02-24	10.0	50CCD	-94.98	1.60 (1.51)	1.92 (1.78)
oelw01010*	16555	2022-02-01	60.0	50CCD	-94.98	1.70 (1.69)	2.04 (2.00)
oelw01020*	16555	2022-02-01	10.0	50CCD	-94.98	1.68 (1.56)	1.99 (1.83)
oelw01030*	16555	2022-02-01	10.0	50CCD	-94.98	1.73 (1.58)	2.08 (1.89)
oelw01040*	16555	2022-02-01	10.0	50CCD	-94.98	1.71 (1.61)	2.01 (1.90)
oelw01050*	16555	2022-02-01	10.0	50CCD	-94.98	1.74 (1.68)	1.97 (1.91)

Table 5. STIS NUV MAMA exposures used in this analysis and their properties. The reference image is indicated with a † symbol.

Exposure	Program ID	Date of Observation	Exposure Time (s)	Aperture	Orientation (PA_APER)	PSF FWHM (Moffat, pix)	PSF FWHM (Gauss, pix)
o40q01a1q	7080	1997-05-26	2300.2	F25CN182	-135.52	2.22	3.01
o46h01ccq	7720	1997-09-29	300.0	F25SRF2	40.26	2.22	2.58
o46h01ceq	7720	1997-09-29	300.0	F25SRF2	40.26	2.05	2.39
o46h01cgq	7720	1997-09-29	355.0	F25SRF2	40.26	1.92	2.56
o46h01ciq	7720	1997-09-29	360.0	F25SRF2	40.27	2.45	3.01
o46h01cmq	7720	1997-09-29	318.0	F25QTZ	40.26	2.15	2.66
o46h01coq	7720	1997-09-29	360.0	F25CN182	40.26	2.18	2.65
o46h02tbq	7720	1998-03-29	314.0	F25SRF2	-139.32	2.28	2.81
o46h02tdq	7720	1998-03-29	360.0	F25SRF2	-139.32	2.42	3.31
o46h02tfq	7720	1998-03-29	360.0	F25SRF2	-139.32	2.86	3.85
o46h02thq	7720	1998-03-29	360.0	F25SRF2	-139.32	2.27	2.89
o46h02tjq	7720	1998-03-29	360.0	F25CN182	-139.32	2.29	2.96
o46h03kbs	7720	1998-09-15	300.0	F25SRF2	37.96	2.13	2.41
o46h03kcq	7720	1998-09-15	300.0	F25SRF2	37.96	2.20	2.60
o46h03keq	7720	1998-09-15	300.0	F25SRF2	37.96	1.74	2.56
o46h03kgq	7720	1998-09-15	300.0	F25SRF2	37.96	2.18	2.54
o46h03kkq	7720	1998-09-15	300.0	F25QTZ	37.96	2.35	2.95
o46h03kmq	7720	1998-09-15	276.0	F25CN182	37.96	2.09	2.63
o46h04f0q	7720	1999-03-24	300.0	F25SRF2	-140.21	2.24	2.66
o46h04f1q	7720	1999-03-24	300.0	F25SRF2	-140.21	2.27	2.84
o46h04f3q	7720	1999-03-24	300.0	F25SRF2	-140.21	2.47	3.32
o46h04f5q	7720	1999-03-24	300.0	F25SRF2	-140.21	2.11	2.60
o46h04f7q	7720	1999-03-24	300.0	F25CN182	-140.21	2.30	2.90
o5in01ssq	8425	1999-09-16	300.0	F25SRF2	38.18	2.13	2.47
o5in01stq	8425	1999-09-16	300.0	F25SRF2	38.18	2.10	2.58
o5in01svq	8425	1999-09-16	300.0	F25SRF2	38.18	1.68	2.52
o5in01sxq	8425	1999-09-16	300.0	F25SRF2	38.18	2.37	2.83
o5in01szq	8425	1999-09-16	300.0	F25QTZ	38.18	2.33	2.79
o5in01t1q	8425	1999-09-16	300.0	F25CN182	38.18	2.26	2.82
o5in01t3q	8425	1999-09-16	300.0	F25SRF2	38.18	2.32	2.80
o5in01t6q	8425	1999-09-16	300.0	F25QTZ	38.18	2.43	3.06
o5in01t7q	8425	1999-09-16	300.0	F25CN182	38.18	2.27	2.59
o5in02cgq	8425	2000-03-27	300.0	F25SRF2	-139.58	2.21	2.65
o5in02chq	8425	2000-03-27	300.0	F25SRF2	-139.58	2.43	3.31
o5in02cjq	8425	2000-03-27	300.0	F25SRF2	-139.58	2.83	3.82
o5in02clq	8425	2000-03-27	300.0	F25SRF2	-139.58	2.21	2.90
o5in02cnq	8425	2000-03-27	300.0	F25QTZ	-139.58	2.63	3.56
o5in02cpq	8425	2000-03-27	300.0	F25CN182	-139.58	2.39	3.40
o5in02crq	8425	2000-03-27	300.0	F25SRF2	-139.58	2.48	3.44
o5in02cuq	8425	2000-03-27	300.0	F25QTZ	-139.58	2.20	2.63
o5in02cvq	8425	2000-03-27	300.0	F25CN182	-139.58	2.22	2.67
o69g01awq	8858	2000-09-18	300.0	F25SRF2	38.51	2.11	2.44

Table 5. (cont'd)

Exposure	Program ID	Date of Observation	Exposure Time (s)	Aperture	Orientation (PA_APER)	PSF FWHM (Moffat, pix)	PSF FWHM (Gauss, pix)
o69g01axq	8858	2000-09-18	300.0	F25SRF2	38.51	2.17	2.56
o69g01azq	8858	2000-09-18	300.0	F25SRF2	38.51	1.85	2.46
o69g01b1q	8858	2000-09-18	300.0	F25SRF2	38.51	2.47	3.12
o69g01b3q	8858	2000-09-18	300.0	F25QTZ	38.51	2.26	2.77
o69g01b5q	8858	2000-09-18	300.0	F25CN182	38.51	2.45	3.10
o69g01b7q	8858	2000-09-18	300.0	F25SRF2	38.51	2.37	2.95
o69g01baq	8858	2000-09-18	300.0	F25QTZ	38.51	2.16	2.46
o69g01bbq	8858	2000-09-18	300.0	F25CN182	38.51	2.02	2.43
o69g02gxq	8858	2001-03-28	300.0	F25SRF2	-139.51	2.68	4.11
o69g02gyq	8858	2001-03-28	300.0	F25QTZ	-139.51	3.22	4.42
o69g02h0q	8858	2001-03-28	300.0	F25CN182	-139.51	2.27	2.70
o69g02h2q	8858	2001-03-28	300.0	F25SRF2	-139.51	2.20	2.78
o69g02h4q	8858	2001-03-28	300.0	F25QTZ	-139.51	2.26	3.03
o69g02h6q	8858	2001-03-28	300.0	F25CN182	-139.51	2.36	3.02
o6i101o6q	8918	2001-09-27	300.0	F25SRF2	39.93	2.46	3.26
o6i101o7q	8918	2001-09-27	300.0	F25SRF2	39.93	2.09	2.42
o6i101o9q	8918	2001-09-27	300.0	F25SRF2	nan	1.12	2.85
o6i101obq	8918	2001-09-27	300.0	F25SRF2	39.94	2.19	2.52
o6i101odq	8918	2001-09-27	300.0	F25QTZ	39.93	2.20	2.52
o6i101ofq	8918	2001-09-27	300.0	F25CN182	39.93	2.26	2.61
o6i101ohq	8918	2001-09-27	300.0	F25SRF2	39.93	2.16	2.49
o6i101okq	8918	2001-09-27	300.0	F25QTZ	39.93	2.70	3.45
o6i101olq	8918	2001-09-27	300.0	F25CN182	39.93	2.46	3.10
o6i102g9q	8918	2002-02-26	300.0	F25SRF2	-144.92	2.36	3.01
o6i102gaq	8918	2002-02-26	300.0	F25QTZ	-144.92	2.53	3.48
o6i102gcq	8918	2002-02-26	300.0	F25CN182	-144.92	2.20	3.08
o6i102geq	8918	2002-02-26	300.0	F25SRF2	-144.92	2.47	3.45
o6i102ggq	8918	2002-02-26	300.0	F25QTZ	-144.92	2.76	3.93
o6i102giq	8918	2002-02-26	300.0	F25CN182	-144.92	2.33	3.49
o8h901vfq	9623	2003-03-27	300.0	F25SRF2	-139.81	2.99	4.14
o8h901vgq	9623	2003-03-27	300.0	F25SRF2	-139.81	3.07	4.92
o8h901vmq	9623	2003-03-27	300.0	F25SRF2	-139.81	2.85	3.82
o8h901voq	9623	2003-03-27	300.0	F25SRF2	-139.81	2.20	2.91
o8h901vqq	9623	2003-03-27	300.0	F25QTZ	-139.81	2.55	3.71
o8h901vsq	9623	2003-03-27	300.0	F25CN182	-139.81	2.37	3.27
o8h901vuq	9623	2003-03-27	300.0	F25SRF2	-139.81	2.63	3.68
o8h901vwq	9623	2003-03-27	300.0	F25QTZ	-139.81	3.13	4.24
o8h901vyq	9623	2003-03-27	300.0	F25CN182	-139.81	2.27	3.46
o8vw01duq	10032	2004-03-04	300.0	F25SRF2	-143.65	2.24	2.63
o8vw01dvq	10032	2004-03-04	300.0	F25SRF2	-143.65	2.01	2.54
o8vw01dxq	10032	2004-03-04	300.0	F25SRF2	-143.65	2.22	2.87
o8vw01dzq	10032	2004-03-04	300.0	F25SRF2	-143.65	2.04	2.45

Table 5. (cont'd)

Exposure	Program ID	Date of Observation	Exposure Time (s)	Aperture	Orientation (PA_APER)	PSF FWHM (Moffat, pix)	PSF FWHM (Gauss, pix)
o8vw01e1q	10032	2004-03-04	300.0	F25QTZ	-143.65	2.19	2.71
o8vw01e3q	10032	2004-03-04	300.0	F25CN182	-143.65	2.19	2.83
o8vw01e5q	10032	2004-03-04	300.0	F25SRF2	-143.65	2.16	2.68
o8vw01e8q	10032	2004-03-04	300.0	F25QTZ	-143.65	2.19	2.65
o8vw01eaq	10032	2004-03-04	300.0	F25CN182	-143.65	2.28	2.63
obav01v9q†	11856	2010-05-06	300.0	F25SRF2	-138.95	2.49	3.02
obav01vaq	11856	2010-05-06	300.0	F25SRF2	-138.95	2.03	2.47
obav01vcq	11856	2010-05-06	300.0	F25SRF2	-138.95	2.18	2.60
obav01veq	11856	2010-05-06	300.0	F25SRF2	-138.95	2.08	2.44
obav01vgq	11856	2010-05-06	300.0	F25QTZ	-138.95	2.22	2.64
obav01viq	11856	2010-05-06	300.0	F25CN182	-138.95	2.26	2.63
obav01vkq	11856	2010-05-06	300.0	F25SRF2	-138.95	2.21	2.63
obav01vmq	11856	2010-05-06	300.0	F25QTZ	-138.95	2.29	2.71
obav01w1q	11856	2010-05-07	300.0	F25CN182	-138.95	2.45	3.06
obmi01xlq	12413	2011-04-16	300.0	F25SRF2	-138.95	2.31	2.73
obmi01xmq	12413	2011-04-16	300.0	F25SRF2	-138.95	2.21	2.68
obmi01xoq	12413	2011-04-16	300.0	F25SRF2	-138.95	2.22	2.87
obmi01xqq	12413	2011-04-16	300.0	F25SRF2	-138.95	2.07	2.45
obmi01xsq	12413	2011-04-16	300.0	F25QTZ	-138.95	2.21	2.69
obmi01xuq	12413	2011-04-16	300.0	F25CN182	-138.95	2.24	2.62
obmi01xwq	12413	2011-04-16	300.0	F25SRF2	-138.95	2.25	2.75
obmi01y0q	12413	2011-04-16	300.0	F25QTZ	-138.95	2.45	2.93
obmi01y2q	12413	2011-04-16	300.0	F25CN182	-138.95	2.37	2.88
obup01rrq	12774	2012-03-14	300.0	F25SRF2	-141.71	2.29	2.74
obup01rsq	12774	2012-03-14	300.0	F25SRF2	-141.71	2.27	2.92
obup01ruq	12774	2012-03-14	300.0	F25SRF2	-141.71	2.40	3.18
obup01rwq	12774	2012-03-14	300.0	F25SRF2	-141.71	2.16	2.60
obup01ryq	12774	2012-03-14	300.0	F25QTZ	-141.71	2.35	3.02
obup01s0q	12774	2012-03-14	300.0	F25CN182	-141.71	2.32	2.90
obup01s2q	12774	2012-03-14	300.0	F25SRF2	-141.71	2.29	2.89
obup01scq	12774	2012-03-14	300.0	F25QTZ	-141.71	2.22	2.64
obup01seq	12774	2012-03-14	300.0	F25CN182	-141.71	2.28	2.71
oc5301h5q	13144	2013-04-13	300.0	F25SRF2	-138.95	2.53	3.10
oc5301h6q	13144	2013-04-13	300.0	F25SRF2	-138.95	2.03	2.43
oc5301h8q	13144	2013-04-13	300.0	F25SRF2	-138.95	2.17	2.51
oc5301haq	13144	2013-04-13	300.0	F25SRF2	-138.95	2.10	2.50
oc5301hcq	13144	2013-04-13	300.0	F25QTZ	-138.95	2.15	2.56
oc5301heq	13144	2013-04-13	300.0	F25CN182	-138.95	2.23	2.72
oc5301hgq	13144	2013-04-13	300.0	F25SRF2	-138.95	2.28	2.69
oc5301hlq	13144	2013-04-13	300.0	F25QTZ	-138.95	2.71	3.50
oc5301hnq	13144	2013-04-13	300.0	F25CN182	-138.95	2.48	3.19
ocff01ryq	13547	2014-04-10	300.0	F25SRF2	-138.95	2.30	2.69

Table 5. (cont'd)

Exposure	Program ID	Date of Observation	Exposure Time (s)	Aperture	Orientation (PA_APER)	PSF FWHM (Moffat, pix)	PSF FWHM (Gauss, pix)
ocff01s0q	13547	2014-04-10	300.0	F25SRF2	-138.95	2.11	2.62
ocff01s2q	13547	2014-04-10	300.0	F25SRF2	-138.95	2.06	2.66
ocff01s4q	13547	2014-04-10	300.0	F25SRF2	-138.95	2.13	2.54
ocff01s6q	13547	2014-04-10	300.0	F25QTZ	-138.95	2.20	2.62
ocff01s8q	13547	2014-04-10	300.0	F25CN182	-138.95	2.31	2.72
ocff01saq	13547	2014-04-10	300.0	F25SRF2	-138.95	2.17	2.59
ocff01sjq	13547	2014-04-10	300.0	F25QTZ	-138.95	2.35	2.80
ocff01slq	13547	2014-04-10	300.0	F25CN182	-138.95	2.28	2.81
ocrk01yuq	13993	2015-04-10	300.0	F25SRF2	-138.95	2.78	3.50
ocrk01yvq	13993	2015-04-10	300.0	F25SRF2	-138.95	2.22	2.67
ocrk01yxq	13993	2015-04-10	300.0	F25SRF2	-138.95	2.08	2.45
ocrk01yzq	13993	2015-04-10	300.0	F25SRF2	-138.95	2.24	2.78
ocrk01z1q	13993	2015-04-10	300.0	F25QTZ	-138.95	2.37	2.89
ocrk01z3q	13993	2015-04-10	300.0	F25CN182	-138.95	2.45	3.05
ocrk01zdq	13993	2015-04-10	300.0	F25CN182	-138.95	2.94	4.08
od1q01mqq	14428	2016-03-26	300.0	F25SRF2	-138.95	2.28	2.77
od1q01mrq	14428	2016-03-26	300.0	F25SRF2	-138.95	2.17	2.60
od1q01mtq	14428	2016-03-26	300.0	F25SRF2	-138.95	2.14	2.70
od1q01mvq	14428	2016-03-26	300.0	F25SRF2	-138.95	2.07	2.42
od1q01mxq	14428	2016-03-26	300.0	F25QTZ	-138.95	2.12	2.53
od1q01mzq	14428	2016-03-26	300.0	F25CN182	-138.95	2.20	2.74
od1q01n1q	14428	2016-03-26	300.0	F25SRF2	-138.95	2.20	2.62
od1q01n5q	14428	2016-03-26	300.0	F25QTZ	-138.95	2.39	2.94
od1q01n8q	14428	2016-03-27	300.0	F25CN182	-138.95	2.43	2.94
odbe01mqq	14832	2017-04-18	300.0	F25SRF2	-138.95	2.38	2.94
odbe01mrq	14832	2017-04-18	300.0	F25SRF2	-138.95	2.15	2.54
odbe01mtq	14832	2017-04-18	300.0	F25SRF2	-138.95	2.24	2.71
odbe01mvq	14832	2017-04-18	300.0	F25SRF2	-138.95	2.11	2.47
odbe01mxq	14832	2017-04-18	300.0	F25QTZ	-138.95	2.21	2.60
odbe01mzq	14832	2017-04-18	300.0	F25CN182	-138.95	2.29	2.81
odbe01n1q	14832	2017-04-18	300.0	F25SRF2	-138.95	2.28	2.68
odbe01nbq	14832	2017-04-19	300.0	F25QTZ	-138.95	2.94	3.87
odbe01ndq	14832	2017-04-19	300.0	F25CN182	-138.95	2.71	3.59
odpg01lcq	14971	2018-04-08	300.0	F25SRF2	-138.95	2.45	2.94
odpg01ldq	14971	2018-04-08	300.0	F25SRF2	-138.95	2.23	2.63
odpg01lfq	14971	2018-04-08	300.0	F25SRF2	-138.95	2.26	2.78
odpg01lhq	14971	2018-04-08	300.0	F25SRF2	-138.95	2.14	2.51
odpg01ljq	14971	2018-04-08	300.0	F25QTZ	-138.95	2.32	2.74
odpg01llq	14971	2018-04-08	300.0	F25CN182	-138.95	2.35	2.82
odpg01lnq	14971	2018-04-08	300.0	F25SRF2	-138.95	2.26	2.69
odpg01lpq	14971	2018-04-08	300.0	F25QTZ	-138.95	2.24	2.63
odpg01lvq	14971	2018-04-08	300.0	F25CN182	-138.95	2.44	3.34

Table 5. (cont'd)

Exposure	Program ID	Date of Observation	Exposure Time (s)	Aperture	Orientation (PA_APER)	PSF FWHM (Moffat, pix)	PSF FWHM (Gauss, pix)
odw501gfq	15560	2019-05-26	300.0	F25SRF2	-138.95	2.71	3.47
odw501ggq	15560	2019-05-26	300.0	F25SRF2	-138.95	2.14	2.54
odw501giq	15560	2019-05-26	300.0	F25SRF2	-138.95	2.12	2.52
odw501gkq	15560	2019-05-26	300.0	F25SRF2	-138.95	2.16	2.55
odw501gmq	15560	2019-05-26	300.0	F25QTZ	-138.95	2.28	2.71
odw501goq	15560	2019-05-26	300.0	F25CN182	-138.95	2.32	2.78
odw501gqq	15560	2019-05-26	300.0	F25SRF2	-138.95	2.31	2.78
odw501gsq	15560	2019-05-26	300.0	F25QTZ	-138.95	2.67	3.41
odw501guq	15560	2019-05-26	300.0	F25CN182	-138.95	2.44	3.12
oe6701q0q	15749	2020-02-26	300.0	F25SRF2	-144.95	2.40	3.01
oe6701q1q	15749	2020-02-26	300.0	F25SRF2	-144.95	2.10	2.48
oe6701q3q	15749	2020-02-26	300.0	F25SRF2	-144.95	2.28	2.64
oe6701q5q	15749	2020-02-26	300.0	F25SRF2	-144.95	2.16	2.59
oe6701q7q	15749	2020-02-26	300.0	F25QTZ	-144.95	2.29	2.69
oe6701q9q	15749	2020-02-26	300.0	F25CN182	-144.95	2.19	2.75
oe6701qbq	15749	2020-02-26	300.0	F25SRF2	-144.95	2.23	2.70
oe6701qjq	15749	2020-02-26	300.0	F25QTZ	-144.95	2.38	2.97
oe6701qlq	15749	2020-02-26	300.0	F25CN182	-144.95	2.37	2.95
oeeh01i4q	16351	2021-02-26	300.0	F25SRF2	-144.80	2.28	2.73
oeeh01i5q	16351	2021-02-26	300.0	F25SRF2	-144.80	2.17	2.66
oeeh01i7q	16351	2021-02-26	300.0	F25SRF2	-144.80	2.28	2.96
oeeh01i9q	16351	2021-02-26	300.0	F25SRF2	-144.80	2.09	2.53
oeeh01ibq	16351	2021-02-26	300.0	F25QTZ	-144.80	2.23	2.94
oeeh01idq	16351	2021-02-26	300.0	F25CN182	-144.80	2.29	2.96
oeeh01ifq	16351	2021-02-26	300.0	F25SRF2	-144.80	2.21	2.88
oeeh01iiq	16351	2021-02-26	300.0	F25QTZ	-144.80	2.15	2.62
oeeh01ikq	16351	2021-02-26	300.0	F25CN182	-144.80	2.36	2.83
oelv01qsq	16554	2022-03-17	300.0	F25SRF2	-138.95	2.32	3.23
oelv01qtq	16554	2022-03-17	300.0	F25SRF2	-138.95	2.86	4.24
oelv01qvq	16554	2022-03-17	300.0	F25SRF2	-138.95	3.12	4.64
oelv01qxq	16554	2022-03-17	300.0	F25SRF2	-138.95	2.32	3.15
oelv01qzq	16554	2022-03-17	300.0	F25QTZ	-138.95	2.71	3.75
oelv01r1q	16554	2022-03-17	300.0	F25CN182	-138.95	2.17	2.90
oelv01r3q	16554	2022-03-17	300.0	F25SRF2	-138.95	2.40	3.40
oelv01r6q	16554	2022-03-17	300.0	F25QTZ	-138.95	2.13	2.61
oelv01r8q	16554	2022-03-17	300.0	F25CN182	-138.95	2.23	2.70

Table 6. STIS FUV MAMA exposures used in this analysis and their properties. The reference image is indicated with a † symbol.

Exposure	Program ID	Date of Observation	Exposure Time (s)	Aperture	Orientation (PA_APER)	PSF FWHM (Moffat, pix)	PSF FWHM (Gauss, pix)
o40q01a5q	7080	1997-05-26	2500.2	F25QTZ	-135.52	2.51	2.96
o40q01a7q	7080	1997-05-26	2600.2	F25SRF2	-135.52	2.55	3.10
o40q02nkq	7080	1997-07-06	1310.8	25MAMA	-20.38	2.21	3.16
o40q02nmq	7080	1997-07-06	429.9	25MAMA	-20.38	1.96	3.45
o40q02noq	7080	1997-07-06	904.3	25MAMA	-20.38	2.21	3.13
o43n01nqq	7132	1997-07-06	300.0	25MAMA	-19.75	2.10	3.15
o43n01nsq	7132	1997-07-06	333.8	25MAMA	-19.75	2.05	3.00
o43n01nuq	7132	1997-07-06	360.0	25MAMA	-19.75	2.24	3.37
o43n01nwq	7132	1997-07-06	360.0	25MAMA	-19.75	2.52	4.15
o43n01nyq	7132	1997-07-06	360.0	25MAMA	-19.75	2.21	5.46
o43n01o0q	7132	1997-07-06	432.0	25MAMA	-19.75	1.50	3.61
o43n01o2q	7132	1997-07-06	432.0	25MAMA	-19.75	2.15	3.25
o43n01o4q	7132	1997-07-06	432.0	25MAMA	-19.75	2.21	3.36
o43n01o6q	7132	1997-07-06	432.0	25MAMA	-19.75	2.41	3.49
o46h01csq	7720	1997-09-29	360.0	25MAMA	40.27	2.07	3.20
o46h01cuq	7720	1997-09-29	360.0	25MAMA	40.26	2.13	3.20
o46h01cyq	7720	1997-09-29	360.0	25MAMA	40.27	0.01	3.68
o46h01d0q	7720	1997-09-29	360.0	F25QTZ	40.26	2.28	2.66
o46h01d2q	7720	1997-09-29	360.0	F25SRF2	40.26	2.23	2.72
o49y01teq	7788	1997-11-06	300.0	25MAMA	47.09	0.09	4.09
o49y01tgq	7788	1997-11-06	400.0	F25SRF2	47.09	2.19	2.65
o46h02tlq	7720	1998-03-29	314.0	25MAMA	-139.32	2.15	3.27
o46h02tnq	7720	1998-03-29	300.0	25MAMA	-139.32	1.99	3.51
o46h02tpq	7720	1998-03-29	300.0	25MAMA	-139.32	0.85	4.02
o46h02trq	7720	1998-03-29	360.0	25MAMA	-139.32	0.01	3.61
o46h02ttq	7720	1998-03-29	360.0	F25QTZ	-139.32	2.28	2.81
o46h03kqq	7720	1998-09-15	300.0	25MAMA	37.96	0.07	4.02
o46h03ksq	7720	1998-09-15	300.0	25MAMA	37.96	0.01	3.25
o46h03kwq	7720	1998-09-15	300.0	25MAMA	37.96	1.84	3.04
o46h03kyq	7720	1998-09-15	300.0	F25QTZ	37.96	2.21	2.67
o46h03l0q	7720	1998-09-15	208.0	F25SRF2	37.96	2.17	2.72
o46h03l3q	7720	1998-09-15	110.4	F25SRF2	37.96	2.17	2.68
o46h04f9q	7720	1999-03-24	300.0	25MAMA	-140.21	0.52	127.27
o46h04fbq	7720	1999-03-24	158.2	25MAMA	-140.21	0.65	142.22
o46h04feq	7720	1999-03-24	170.1	25MAMA	-140.21	0.79	153.76
o46h04ffq	7720	1999-03-24	360.0	25MAMA	-140.21	2.05	3.04
o46h04fhq	7720	1999-03-24	360.0	25MAMA	-140.21	1.86	2.95
o46h04fjq	7720	1999-03-24	360.0	F25QTZ	-140.21	2.12	2.52
o5in01t9q	8425	1999-09-17	400.0	25MAMA	38.18	0.07	3.98
o5in01tbq	8425	1999-09-17	400.0	25MAMA	38.18	0.01	4.17
o5in01tfq	8425	1999-09-17	400.0	25MAMA	38.18	1.74	3.21
o5in01tiq	8425	1999-09-17	400.0	F25QTZ	38.18	2.25	2.78

Table 6. (cont'd)

Exposure	Program ID	Date of Observation	Exposure Time (s)	Aperture	Orientation (PA_APER)	PSF FWHM (Moffat, pix)	PSF FWHM (Gauss, pix)
o5in01tjq	8425	1999-09-17	400.0	F25SRF2	38.18	1.93	2.80
o5in01tlq	8425	1999-09-17	400.0	25MAMA	38.18	0.10	4.38
o5in01tnq	8425	1999-09-17	400.0	F25QTZ	38.18	2.10	2.47
o5in01tpq	8425	1999-09-17	400.0	F25SRF2	38.18	2.19	2.69
o5in02cxq	8425	2000-03-27	400.0	25MAMA	-139.58	0.01	3.82
o5in02czq	8425	2000-03-27	400.0	25MAMA	-139.58	0.16	105.27
o5in02d1q	8425	2000-03-27	400.0	25MAMA	-139.58	0.12	82.70
o5in02d3q	8425	2000-03-27	400.0	25MAMA	-139.58	0.51	104.26
o5in02d6q	8425	2000-03-27	400.0	F25QTZ	-139.58	2.17	2.58
o5in02d7q	8425	2000-03-27	400.0	F25SRF2	-139.58	2.19	2.72
o5in02d9q	8425	2000-03-27	400.0	25MAMA	-139.58	0.01	4.21
o5in02dbq	8425	2000-03-27	400.0	F25QTZ	-139.58	2.51	3.15
o5in02ddq	8425	2000-03-27	400.0	F25SRF2	-139.58	1.88	3.47
o69g01bdq	8858	2000-09-18	400.0	25MAMA	38.51	0.01	3.32
o69g01bfq	8858	2000-09-18	400.0	25MAMA	38.51	0.78	3.19
o69g01bhq	8858	2000-09-18	400.0	25MAMA	38.51	1.75	3.46
o69g01bjq	8858	2000-09-18	400.0	25MAMA	38.51	1.65	2.83
o69g01bmq	8858	2000-09-18	400.0	F25QTZ	38.51	2.32	2.73
o69g01bnq	8858	2000-09-18	400.0	F25SRF2	38.51	2.21	2.77
o69g01bpq	8858	2000-09-18	400.0	25MAMA	38.51	0.02	3.28
o69g01brq	8858	2000-09-18	400.0	F25QTZ	38.51	2.12	2.61
o69g01btq	8858	2000-09-18	400.0	F25SRF2	38.51	2.20	2.68
o69g02h8q	8858	2001-03-28	197.0	25MAMA	-139.51	0.14	4.63
o69g02hbq	8858	2001-03-28	203.0	25MAMA	-139.51	0.50	147.19
o69g02hcq	8858	2001-03-28	400.0	F25QTZ	-139.51	2.56	3.19
o69g02heq	8858	2001-03-28	400.0	F25SRF2	-139.51	0.01	3.73
o69g02hgq	8858	2001-03-28	400.0	25MAMA	-139.51	1.75	3.31
o69g02hiq	8858	2001-03-28	400.0	F25QTZ	-139.51	2.23	2.76
o69g02hkq	8858	2001-03-28	153.0	F25SRF2	-139.51	2.24	2.79
o69g02hnq	8858	2001-03-28	247.0	F25SRF2	-139.51	2.29	2.94
o6i101onq	8918	2001-09-27	400.0	25MAMA	39.94	0.01	4.71
o6i101opq	8918	2001-09-27	400.0	25MAMA	39.93	0.01	3.62
o6i101orq	8918	2001-09-27	400.0	25MAMA	39.93	0.04	2.83
o6i101otq	8918	2001-09-27	400.0	25MAMA	39.94	0.05	3.33
o6i101owq	8918	2001-09-27	400.0	F25QTZ	39.93	3.07	3.77
o6i101oxq	8918	2001-09-27	400.0	F25SRF2	39.93	2.68	3.78
o6i101ozq	8918	2001-09-27	400.0	25MAMA	39.94	0.01	4.02
o6i101p1q	8918	2001-09-27	400.0	F25QTZ	39.93	2.37	2.79
o6i101p3q	8918	2001-09-27	400.0	F25SRF2	39.93	2.25	2.79
o6i102gkq	8918	2002-02-26	198.0	25MAMA	-144.92	1.35	180.86
o6i102gmq	8918	2002-02-26	202.0	25MAMA	-144.92	1.68	178.92
o6i102goq	8918	2002-02-26	400.0	F25QTZ	-144.92	2.24	2.72

Table 6. (cont'd)

Exposure	Program ID	Date of Observation	Exposure Time (s)	Aperture	Orientation (PA_APER)	PSF FWHM (Moffat, pix)	PSF FWHM (Gauss, pix)
o6i102gqq	8918	2002-02-26	400.0	F25SRF2	-144.92	2.29	2.85
o6i102gsq	8918	2002-02-26	400.0	25MAMA	-144.92	0.21	5.87
o6i102guq	8918	2002-02-26	400.0	F25QTZ	-144.92	2.77	3.43
o6i102gwq	8918	2002-02-26	155.0	F25SRF2	-144.92	1.93	3.67
o6i102gyq	8918	2002-02-26	245.0	F25SRF2	-144.92	1.88	3.86
o8h901w0q	9623	2003-03-27	400.0	25MAMA	-139.81	0.64	152.87
o8h901w5q	9623	2003-03-27	400.0	25MAMA	-139.81	2.17	3.66
o8h901w7q	9623	2003-03-27	400.0	25MAMA	-139.81	1.81	4.42
o8h901w9q	9623	2003-03-27	400.0	25MAMA	-139.81	0.01	3.87
o8h901wbq	9623	2003-03-27	400.0	F25QTZ	-139.81	2.69	3.33
o8h901wdq	9623	2003-03-27	400.0	F25SRF2	-139.81	2.42	3.37
o8h901wfq	9623	2003-03-27	400.0	25MAMA	-139.81	0.63	141.13
o8h901wkq	9623	2003-03-27	400.0	F25QTZ	-139.81	2.24	2.78
o8h901wmq	9623	2003-03-27	400.0	F25SRF2	-139.81	2.29	2.93
o8vw01efq	10032	2004-03-04	400.0	25MAMA	-143.65	0.01	4.23
o8vw01ehq	10032	2004-03-04	400.0	25MAMA	-143.65	0.49	124.79
o8vw01ejq	10032	2004-03-04	400.0	25MAMA	-143.65	0.33	95.36
o8vw01eoq	10032	2004-03-04	400.0	25MAMA	-143.65	0.29	97.77
o8vw01exq	10032	2004-03-04	400.0	F25QTZ	-143.65	2.25	2.67
o8vw01f2q	10032	2004-03-04	400.0	F25SRF2	-143.65	2.26	2.76
o8vw01f4q	10032	2004-03-04	400.0	25MAMA	-143.65	0.12	4.26
o8vw01f6q	10032	2004-03-04	400.0	F25QTZ	-143.65	2.17	2.62
o8vw01fbq	10032	2004-03-04	400.0	F25SRF2	-143.65	2.15	2.72
obav01w4q†	11856	2010-05-07	400.0	25MAMA	-138.95	2.16	3.56
obav01w6q	11856	2010-05-07	400.0	25MAMA	-138.95	1.87	3.18
obav01w8q	11856	2010-05-07	400.0	25MAMA	-138.95	0.01	3.24
obav01waq	11856	2010-05-07	400.0	25MAMA	-138.95	0.01	3.48
obav01wdq	11856	2010-05-07	400.0	F25QTZ	-138.95	2.14	2.52
obav01wpq	11856	2010-05-07	400.0	F25SRF2	-138.95	2.91	3.47
obav01wtq	11856	2010-05-07	400.0	25MAMA	-138.95	1.83	3.56
obav01wwq	11856	2010-05-07	400.0	F25QTZ	-138.95	2.12	2.52
obav01wzq	11856	2010-05-07	400.0	F25SRF2	-138.95	2.21	2.73
obmi01y4q	12413	2011-04-16	400.0	25MAMA	-138.95	1.61	3.55
obmi01y6q	12413	2011-04-16	400.0	25MAMA	-138.95	0.01	3.35
obmi01y8q	12413	2011-04-16	400.0	25MAMA	-138.95	0.01	3.67
obmi01yaq	12413	2011-04-16	400.0	25MAMA	-138.95	0.10	4.04
obmi01yeq	12413	2011-04-16	400.0	F25QTZ	-138.95	2.73	3.23
obmi01ygq	12413	2011-04-16	400.0	F25SRF2	-138.95	2.40	3.03
obmi01yiq	12413	2011-04-16	400.0	25MAMA	-138.95	0.01	3.51
obmi01ykq	12413	2011-04-16	400.0	F25QTZ	-138.95	2.16	2.57
obmi01ymq	12413	2011-04-16	400.0	F25SRF2	-138.95	2.12	2.65
obup01sgq	12774	2012-03-14	400.0	25MAMA	-141.71	0.01	3.70

Table 6. (cont'd)

Exposure	Program ID	Date of Observation	Exposure Time (s)	Aperture	Orientation (PA_APER)	PSF FWHM (Moffat, pix)	PSF FWHM (Gauss, pix)
obup01siq	12774	2012-03-14	400.0	25MAMA	-141.71	0.01	3.71
obup01skq	12774	2012-03-14	400.0	25MAMA	-141.71	0.36	5.17
obup01smq	12774	2012-03-14	400.0	25MAMA	-141.71	0.39	110.25
obup01stq	12774	2012-03-14	400.0	F25QTZ	-141.71	2.20	2.60
obup01svq	12774	2012-03-14	400.0	F25SRF2	-141.71	2.14	2.64
obup01sxq	12774	2012-03-14	400.0	25MAMA	-141.71	0.01	3.87
obup01szq	12774	2012-03-14	400.0	F25QTZ	-141.71	2.27	2.71
obup01t1q	12774	2012-03-14	400.0	F25SRF2	-141.71	2.03	2.75
oc5301hpq	13144	2013-04-13	400.0	25MAMA	-138.95	1.23	3.97
oc5301hrq	13144	2013-04-13	400.0	25MAMA	-138.95	0.01	3.55
oc5301htq	13144	2013-04-13	400.0	25MAMA	-138.95	0.01	3.67
oc5301hvq	13144	2013-04-13	400.0	25MAMA	-138.95	0.29	97.97
oc5301i0q	13144	2013-04-13	400.0	F25QTZ	-138.95	3.36	3.92
oc5301i2q	13144	2013-04-13	400.0	F25SRF2	-138.95	3.09	3.61
oc5301i4q	13144	2013-04-13	400.0	25MAMA	-138.95	0.01	3.98
oc5301i6q	13144	2013-04-13	400.0	F25QTZ	-138.95	2.27	2.69
oc5301i8q	13144	2013-04-13	400.0	F25SRF2	-138.95	2.14	2.83
ocff01snq	13547	2014-04-10	400.0	25MAMA	-138.95	0.01	3.83
ocff01spq	13547	2014-04-10	400.0	25MAMA	-138.95	0.08	3.75
ocff01t3q	13547	2014-04-10	400.0	25MAMA	-138.95	0.14	4.25
ocff01t5q	13547	2014-04-10	400.0	25MAMA	-138.95	0.31	106.09
ocff01tkq	13547	2014-04-10	400.0	F25QTZ	-138.95	2.42	2.89
ocff01tmq	13547	2014-04-10	400.0	F25SRF2	-138.95	2.27	2.80
ocff01tpq	13547	2014-04-10	400.0	25MAMA	-138.95	0.01	3.94
ocff01trq	13547	2014-04-10	400.0	F25QTZ	-138.95	2.14	2.55
ocff01ttq	13547	2014-04-10	400.0	F25SRF2	-138.95	2.00	2.74
ocrk01zfq	13993	2015-04-10	400.0	25MAMA	-138.95	0.97	5.02
ocrk01zhq	13993	2015-04-10	400.0	25MAMA	-138.95	0.01	3.98
ocrk01zjq	13993	2015-04-10	400.0	25MAMA	-138.95	0.23	4.33
ocrk01zlq	13993	2015-04-10	400.0	25MAMA	-138.95	0.31	116.19
ocrk01znq	13993	2015-04-10	400.0	F25QTZ	-138.95	5.26	5.48
ocrk01zpq	13993	2015-04-10	400.0	F25SRF2	-138.95	4.46	5.00
ocrk01zrq	13993	2015-04-10	400.0	25MAMA	-138.95	2.01	5.03
ocrk01ztq	13993	2015-04-10	400.0	F25QTZ	-138.95	2.56	3.26
ocrk01zvq	13993	2015-04-10	400.0	F25SRF2	-138.95	2.80	3.87
od1q01naq	14428	2016-03-27	400.0	25MAMA	-138.95	0.01	3.67
od1q01ncq	14428	2016-03-27	400.0	25MAMA	-138.95	0.01	3.40
od1q01nfq	14428	2016-03-27	400.0	25MAMA	-138.95	0.01	3.75
od1q01nhq	14428	2016-03-27	400.0	25MAMA	-138.95	0.36	101.50
od1q01nkq	14428	2016-03-27	400.0	F25QTZ	-138.95	2.58	3.07
od1q01nmq	14428	2016-03-27	400.0	F25SRF2	-138.95	2.43	2.98
od1q01noq	14428	2016-03-27	400.0	25MAMA	-138.95	0.01	3.88

Table 6. (cont'd)

Exposure	Program ID	Date of Observation	Exposure Time (s)	Aperture	Orientation (PA_APER)	PSF FWHM (Moffat, pix)	PSF FWHM (Gauss, pix)
od1q01nqq	14428	2016-03-27	400.0	F25QTZ	-138.95	2.24	2.67
od1q01nsq	14428	2016-03-27	400.0	F25SRF2	-138.95	2.22	2.81
odbea1flq	14832	2017-06-09	400.0	25MAMA	-138.95	3.67	5.79
odbea1fmq	14832	2017-06-09	400.0	25MAMA	-138.95	2.44	3.81
odbea1foq	14832	2017-06-09	400.0	25MAMA	-138.95	2.07	3.12
odbea1fqq	14832	2017-06-09	400.0	25MAMA	-138.95	2.36	3.89
odbea1fsq	14832	2017-06-09	400.0	F25QTZ	-138.95	2.70	3.21
odbea1fuq	14832	2017-06-09	400.0	F25SRF2	-138.95	5.90	6.56
odbea1fwq	14832	2017-06-09	400.0	25MAMA	-138.95	3.54	5.10
odbea1fyq	14832	2017-06-09	400.0	F25QTZ	-138.95	3.10	3.70
odbea1g0q	14832	2017-06-09	400.0	F25SRF2	-138.95	3.22	3.68
odpg01lxq	14971	2018-04-08	400.0	25MAMA	-138.95	3.07	4.06
odpg01lzq	14971	2018-04-08	400.0	25MAMA	-138.95	2.17	3.40
odpg01m1q	14971	2018-04-08	400.0	25MAMA	-138.95	1.93	3.21
odpg01m3q	14971	2018-04-08	400.0	25MAMA	-138.95	0.01	3.64
odpg01m6q	14971	2018-04-08	400.0	F25QTZ	-138.95	2.45	2.89
odpg01mfq	14971	2018-04-08	400.0	F25SRF2	-138.95	4.12	4.66
odpg01mhq	14971	2018-04-08	400.0	25MAMA	-138.95	3.03	4.25
odpg01mjq	14971	2018-04-08	400.0	F25QTZ	-138.95	2.75	3.19
odpg01mlq	14971	2018-04-08	400.0	F25SRF2	-138.95	2.60	3.19
odw501gwq	15560	2019-05-26	400.0	25MAMA	-138.95	2.47	3.55
odw501gyq	15560	2019-05-26	400.0	25MAMA	-138.95	2.14	3.06
odw501h0q	15560	2019-05-26	400.0	25MAMA	-138.95	1.92	3.51
odw501h2q	15560	2019-05-26	400.0	25MAMA	-138.95	0.01	3.20
odw501h4q	15560	2019-05-26	400.0	F25QTZ	-138.95	3.05	3.73
odw501h6q	15560	2019-05-26	400.0	F25SRF2	-138.95	2.77	3.43
odw501h8q	15560	2019-05-26	400.0	25MAMA	-138.95	2.42	3.47
odw501haq	15560	2019-05-26	400.0	F25QTZ	-138.95	2.31	2.77
odw501hcq	15560	2019-05-26	400.0	F25SRF2	-138.95	2.14	2.65
oe6701qnq	15749	2020-02-26	400.0	25MAMA	-144.95	0.10	4.48
oe6701qpq	15749	2020-02-26	400.0	25MAMA	-144.95	0.14	3.99
oe6701qrq	15749	2020-02-26	400.0	25MAMA	-144.95	0.15	101.67
oe6701qtq	15749	2020-02-26	400.0	25MAMA	-144.95	0.43	105.14
oe6701qvq	15749	2020-02-26	400.0	F25QTZ	-144.95	2.42	2.98
oe6701qxq	15749	2020-02-26	400.0	F25SRF2	-144.95	2.23	3.01
oe6701qzq	15749	2020-02-26	400.0	25MAMA	-144.95	0.23	5.04
oe6701r1q	15749	2020-02-26	400.0	F25QTZ	-144.95	2.27	2.71
oe6701r3q	15749	2020-02-26	400.0	F25SRF2	-144.95	2.32	2.91
oeeh01imq	16351	2021-02-26	400.0	25MAMA	-144.80	0.02	4.15
oeeh01ipq	16351	2021-02-27	400.0	25MAMA	-144.80	0.43	127.97
oeeh01irq	16351	2021-02-27	400.0	25MAMA	-144.80	0.32	89.48
oeeh01iuq	16351	2021-02-27	400.0	25MAMA	-144.80	0.45	100.56

Table 6. (cont'd)

Exposure	Program ID	Date of Observation	Exposure Time (s)	Aperture	Orientation (PA_APER)	PSF FWHM (Moffat, pix)	PSF FWHM (Gauss, pix)
oeeh01ixq	16351	2021-02-27	400.0	F25QTZ	-144.80	2.20	2.57
oeeh01izq	16351	2021-02-27	400.0	F25SRF2	-144.80	2.14	2.64
oeeh01j1q	16351	2021-02-27	400.0	25MAMA	-144.80	0.10	121.53
oeeh01j3q	16351	2021-02-27	400.0	F25QTZ	-144.80	2.28	2.80
oeeh01j5q	16351	2021-02-27	400.0	F25SRF2	-144.80	2.17	2.81
oelv01raq	16554	2022-03-17	400.0	25MAMA	-138.95	0.01	3.67
oelv01rdq	16554	2022-03-17	400.0	25MAMA	-138.95	0.13	109.51
oelv01rfq	16554	2022-03-17	400.0	25MAMA	-138.95	0.01	5.74
oelv01rhq	16554	2022-03-17	400.0	25MAMA	-138.95	0.40	108.51
oelv01rkq	16554	2022-03-17	400.0	F25QTZ	-138.95	2.20	2.63
oelv01rmq	16554	2022-03-17	400.0	F25SRF2	-138.95	2.12	2.62
oelv01roq	16554	2022-03-17	400.0	25MAMA	-138.95	0.07	4.10
oelv01rqq	16554	2022-03-17	400.0	F25QTZ	-138.95	2.34	2.82
oelv01rsq	16554	2022-03-17	400.0	F25SRF2	-138.95	1.98	2.73